Hindawi
International Journal of Aerospace Engineering
Volume 2020, Article ID 6515626, 16 pages
https://doi.org/10.1155/2020/6515626

Research Article

Adaptive Neural Network Variable Structure Control for Liquid-Filled Spacecraft under Unknown Input Saturation

Hongwei Wang,[1] Shufeng Lu,[2] and Xiaojuan Song[1]

[1]*College of Mechanical Engineering, Inner Mongolia University of Technology, Hohhot 010051, China*
[2]*Department of Mechanics, Inner Mongolia University of Technology, Hohhot 010051, China*

Correspondence should be addressed to Xiaojuan Song; xjsong0603@163.com

Received 30 January 2020; Revised 17 July 2020; Accepted 28 July 2020; Published 1 September 2020

Academic Editor: Christian Circi

Copyright © 2020 Hongwei Wang et al. This is an open access article distributed under the Creative Commons Attribution License, which permits unrestricted use, distribution, and reproduction in any medium, provided the original work is properly cited.

This study addresses the problem of attitude maneuver control for a three-axis stabilized liquid-filled spacecraft using an adaptive neural network variable structure control algorithm in the presence of parametric uncertainty, external disturbances, and control input saturation. The liquid fuel is equivalent to a spherical pendulum model, and the coupled dynamic model of liquid-filled spacecraft is derived using the conservation law of angular momentum moment. Then, adaptive variable structure control technique is designed, which contains hyperbolic tangent function that preserves control smoothness at all times. The proposed control algorithm has the properties that state variables converge to the origin asymptotically under parametric uncertainty and external disturbance. Furthermore, the controller derived here is extended by adding a feed-forward saturation compensation scheme to reduce the influence of unknown control input saturation on the system. Also, the saturation compensation scheme is derived by using a radial basis function neural network to approximate the unknown saturation nonlinearity. The associated stability proof of the resulting closed-loop system is presented based on Lyapunov analysis, and asymptotic convergence of the state variables is guaranteed via the Barbalat lemma. Numerical simulations are presented to illustrate the spacecraft performance obtained by using the proposed controllers.

1. Introduction

Modern spacecraft often contain large amounts of liquid fuel to achieve highly accurate pointing, fast slewing, and other fast maneuvers from large initial conditions during orbital transfer, rendezvous, and docking. Understanding the coupling effect between the sloshing dynamics of the fuel and a vehicle's control systems is one of the major challenges for the aerospace industry. Liquid sloshing is usually considered to be the motion of the liquid surface inside its container. When a spacecraft with partially filled liquid performs attitude or trajectory maneuvers, liquid fuel in the tank inevitably sloshes. Liquid sloshing often has a significant impact on spacecraft attitude as well as can even induce instability and gives a great challenge to the design of controller with high precision [1–3]. Taking the famous SpaceX Falcon 1 in 2007 as an example, the fuel slosh caused by its second stage spin is out of control. Fuel sloshing can affect the dynamic response, which leads to mass distribution and energy dissipation. In order to reduce these effects and design high-performance controllers for liquid-filled spacecraft, it is necessary to study the coupled model and controller design for liquid-filled spacecraft. Many researchers have studied the effects of liquid sloshing on spacecraft attitude control systems. In the control system, a linear equivalent mechanical model (EMM), such as a pendulum model and a spring-mass model, is often used to replace liquid sloshing [2, 4]. Yue [5] studied the chaotic dynamics of a flexible spacecraft with a liquid-filled tank, where the liquid sloshing inside the tank was represented by a pendulum model [6]. Yue and Zhu [7] employed the equivalent spherical pendulum model to derive a mathematical model of a spacecraft and designed a hybrid control method based on input shaping technology and feedback linearization method to control the implementation of an attitude maneuver. With consideration of parameter uncertainties and unknown external disturbances, Song and Lu [8] used a two-mode spring-mass model to establish a mathematical model for the liquid-

filled spacecraft, and a hybrid control method was developed by combining adaptive sliding mode control with the input shaping technology to achieve the attitude maneuver task. Zhang and Wang [9] studied the attitude regulation of a liquid-filled spacecraft under low-frequency sinusoidal disturbances. The dynamic model of the liquid-filled spacecraft was represented by a rigid body with a single spherical pendulum. Kang and Cochran [10] treated the sloshing mass of a spacecraft inside a partially filled liquid tank as a spherical pendulum model and investigated the problem of control stability of a spinning spacecraft. Among these equivalent models, the pendulum model is more suitable and is widely used in the study of launch vehicles. In this paper, the sloshing dynamics are modeled by a simple pendulum.

Variable structure control (VSC) has been extensively investigated in the design of robust controllers with high accuracy for linear and nonlinear systems and has been applied to various engineering fields. This usage is due to the fact that VSC has the advantage of dealing with unknown external disturbances, model uncertainties, and fast dynamic control for dynamic systems. For these advantages, VSC has received growing attention in the field of spacecraft attitude control research [11–16]. Boškovic et al. [11] proposed two globally stable VSC algorithms for robust stabilization of rigid spacecraft under control input saturation, parametric uncertainty, and external disturbances. Wallsgrove and Akella [12] developed a globally stabilizing saturated VSC for a rigid spacecraft with unknown bounded disturbances. VSC also provides a systematic approach to the design of on/off control laws for multivariable systems, which is a desirable approach for the thruster-actuator modes commonly used in satellites. However, since variable structure controllers usually use high-frequency switching to drive the trajectories of the system on the sliding surface, this inevitably results in the chattering of the signal in the system in practical applications. Therefore, it is necessary to eliminate this undesirable characteristic by replacing the sign function with a saturation function in the design of such a controller [17–19].

An important problem encountered in practice is the limitations of control inputs because of the physical constraints of onboard actuators. Input magnitude saturation is one of the major control issues in spacecraft attitude control systems, and the occurrence of input saturation may lead to unacceptable performance degradation or even instability. The design of controllers with input saturation has both practical interest and theoretical significance. This is a challenging problem since the input magnitude is upper-bounded by a priori fixed constant. Some researchers have solved the attitude control problem with actuator saturation. Zou and Kumar [20] proposed a robust adaptive fuzzy controller for spacecraft in the presence of unknown mass moment of inertia matrix, external disturbances, actuator failure, and control input constraints. Zou and Kumar [21] considered the problem of the control input saturation and proposed a distributed attitude coordination control scheme for spacecraft formation flying based on a neural network. Zhu et al. [22] presented an adaptive sliding mode controller for the attitude stabilization of spacecraft under control constraints. Ma et al. [23] proposed a fault-tolerant attitude tracking control scheme for a flexible spacecraft under actuator failure, model uncertainty, external disturbances, and actuator saturation. In addition, the authors of [24–26] proposed a novel saturation compensation scheme for nonlinear systems based on a radial basis function (RBF) neural network. This method uses a smooth function to approximate the saturation function, and an RBF neural network is employed to approximate unknown control input saturation. Based on the RBF neural network, a feed-forward saturation compensator is developed to reduce the influence of unknown input saturation for spacecraft in [27, 28].

Inspired by the aforementioned works, in this work, the problem of the attitude maneuver of a liquid-filled spacecraft is investigated under input saturation, parametric uncertainty, and external disturbances. Variable structure control (VSC) and adaptive control approaches are applied to design the control algorithms. The main elements of this paper are stated as follows:

(1) The dynamic equation of a three-axis stabilized liquid-filled spacecraft is established by using the law of conservation of momentum, and the liquid fuel inside the partially filled fuel tank is modeled as a spherical pendulum

(2) A continuous hyperbolic tangent function is incorporated into the design of the controller, rather than the typical switching function of variable structure control, to ensure control signal smoothness at all times. Based on the RBF neural network, an actuator saturation compensation scheme is presented to compensate for the effects of input saturation on the spacecraft attitude control system

(3) State variables of the system converge to the origin asymptotically by the proposed controller under parametric uncertainty and external disturbances. Also, the corresponding control torque converge to the origin subject to input saturation

The remainder of this paper is organized as follows. In Section 2, the mathematical model of the liquid-filled spacecraft is established, and the attitude control problem is formulated. Subsequently, the adaptive output feedback VSC is proposed, and a rigorous stability analysis of the resulting closed-loop system is presented in Section 3. Simulation results are then presented and analysed in Section 4 followed by conclusions in Section 5.

2. Mathematical Modelling

The mathematical model of rigid-liquid coupling spacecraft can be described by the following dynamic and kinematic equations.

2.1. The Dynamic Equation. As shown in Figure 1, the inertial coordinate frame is indicated by $O-XYZ$. The body-fixed coordinate frame is indicted by $O_1-X_1Y_1Z_1$; the point O_1 represents the center mass of the rigid body of the spacecraft.

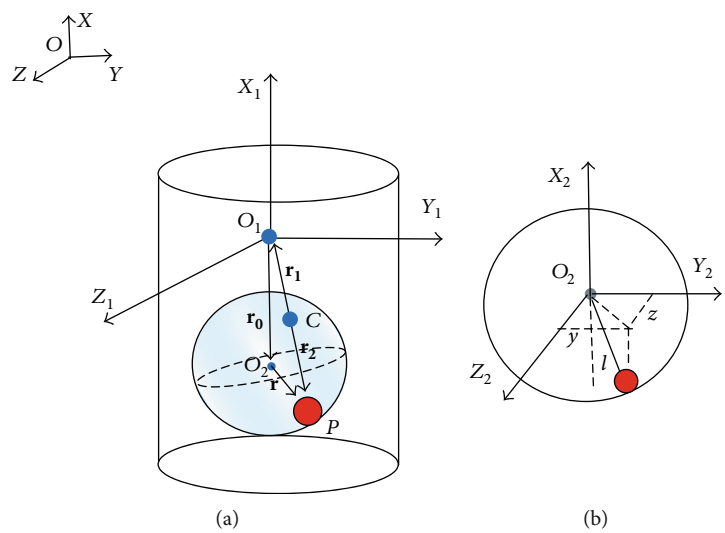

Figure 1: Schematic diagram and dynamic model of liquid-filled spacecraft. (a) Simplified schematic diagram. (b) Equivalent model of liquid sloshing.

And the spherical pendulum coordinate frame is indicated by $O_2 - X_2Y_2Z_2$. The pivot point (or attachment point) of the spherical pendulum is represented by point O_2, which is located on the O_1X_1 axis of the spacecraft body-fixed coordinate frame. The length of the spherical pendulum is represented by l, point C represents the centers of masses of the system, and point P represents the position of the spherical pendulum.

In view of the limitation of the length of the pendulum and the size of the tank, the sloshing of the liquid fuel is assumed to a small amplitude, namely, y, $z < < l$, such that $x \approx -l$. The location of point P with respect to O_2 can be expressed as

$$\mathbf{r} = \left[-\sqrt{l^2 - y^2 - z^2}\, y\, z\right]^{\mathrm{T}} = [-l \quad y \quad z]^{\mathrm{T}}. \tag{1}$$

The angular momentum of the system about point C can be written as

$$\mathbf{H} = \mathbf{J}\boldsymbol{\omega} + \mu m_b \mathbf{r}_p{}^{\times}\left(\boldsymbol{\omega}^{\times}\mathbf{r}_p + \dot{\mathbf{r}}_p\right), \tag{2}$$

where $\mu = m_b/(m_b + m_b)$, m_b and m_p represent the masses of spacecraft main body and spherical pendulum, respectively.

As such, equation (2) can be written as matrix form

$$\mathbf{H} = \mathbf{J}_b\boldsymbol{\omega} + \mathbf{h}_p, \tag{3}$$

where $\mathbf{J}_b = \mathbf{J} - \mu \mathrm{m}_b \mathbf{r_p}{}^{\times}\mathbf{r_p}{}^{\times}$, $\mathbf{h_p} = \mu \mathrm{m}_b \mathbf{r_p}{}^{\times}\dot{\mathbf{r}}$.

The law of conservation of angular momentum is applied to equation (3), and the kinetic equations of the system can be written as

$$\mathbf{J}_b\dot{\boldsymbol{\omega}} + \boldsymbol{\delta}^{\mathrm{T}}\ddot{\boldsymbol{\eta}} = -\boldsymbol{\omega}^{\times}\left(\mathbf{J}_b\boldsymbol{\omega} + \boldsymbol{\delta}^{\mathrm{T}}\dot{\boldsymbol{\eta}}\right) - \mathbf{J}_b\boldsymbol{\omega} + \mathbf{d}(t) + \mathbf{u}. \tag{4}$$

where

$$\boldsymbol{\delta} = \mu m_b \begin{bmatrix} -z & 0 & r_x - l \\ y & -(r_x - l) & 0 \end{bmatrix}, \tag{5}$$

r_x represents the distance between point O_1 and point O_2. $\boldsymbol{\eta} = [y \quad z]^{\mathrm{T}}$ indicates the sloshing variable of the spherical pendulum.

The dynamic equation for the relative motion of the pendulum is derived under the assumption that point C is stationary in space. Therefore, the dynamic equation of the pendulum about point C can be written as

$$\mu m_b \mathbf{a_p} = \mathbf{T_o} + \mathbf{T_g}, \tag{6}$$

where $\mathbf{a_p} = \ddot{\mathbf{r}}_2 = (1 - \mu)\ddot{\mathbf{r}}_\mathbf{p}$ denotes the absolute acceleration of point P, and $\ddot{\mathbf{r}}_\mathbf{p} = \ddot{\mathbf{r}} + \dot{\boldsymbol{\omega}}^{\times}\mathbf{r_p} + 2\boldsymbol{\omega}^{\times}\dot{\mathbf{r}} + \boldsymbol{\omega}^{\times}(\boldsymbol{\omega}^{\times}\mathbf{r_p})$, $\mathbf{T_0} = -[\partial R/\partial \dot{y} \quad \partial R/\partial \dot{z}]^{\mathrm{T}}$ with $R = c_1\dot{y}^2 + c_2\dot{z}^2 (\dot{y}, \dot{z} \neq 0)$, in which c_1 and c_2 represent the viscosity coefficients of liquid fuel. $\mathbf{T_g} = [\partial U/\partial \mathrm{y} \quad \partial U/\partial \mathrm{z}]^{\mathrm{T}}$ with $U = m_p g\sqrt{l^2 - y^2 - z^2}$.

2.2. The Kinematic Equation. In order to avoid the singularity of parameters, the familiar four unitary quaternions $[q_0 \quad \mathbf{q}]^{\mathrm{T}} \in R^4$ is employed to describe the attitude of the spacecraft as follows:

$$\begin{bmatrix} \dot{q}_0 \\ \dot{\mathbf{q}} \end{bmatrix} = \frac{1}{2}\mathbf{S}^{\mathrm{T}}(q_0, \mathbf{q})\boldsymbol{\omega} = \frac{1}{2}\begin{bmatrix} -\mathbf{q} \\ q_0\mathbf{I}_3 + \mathbf{q}^{\times} \end{bmatrix}\boldsymbol{\omega}, \tag{7}$$

where $\boldsymbol{\omega} \in R^3$ represents the angular velocity of the spacecraft. $\mathbf{q}^{\times} \in R^{3\times 3}$ denotes the skew symmetric matrix of $\mathbf{q}$. The four unitary quaternions are subjecting to the constraint relationship $q_0{}^2 + \mathbf{q}^{\mathrm{T}}\mathbf{q} = 1$.

Here, the sloshing of the liquid is assumed to be negligibly small. Hence, the second-order small quantities in the

dynamic system coupling equations (equations (4) and (6)) can be neglected for linearization. As a result, the new vector matrix $\boldsymbol{\psi}$ is introduced for convenience in equation (6). Finally, it is possible to obtain the mathematical model of the liquid-filled spacecraft as follows:

$$\mathbf{J}_{mb}\dot{\boldsymbol{\omega}} = -\boldsymbol{\omega}^{\times}\left(\mathbf{J}_{mb}\boldsymbol{\omega} + \boldsymbol{\delta}^{\mathrm{T}}\boldsymbol{\psi}\right) + \boldsymbol{\delta}^{\mathrm{T}}\left(\mathbf{C}\boldsymbol{\psi} + \mathbf{K}\boldsymbol{\eta} - \mathbf{C}\mathbf{M}^{-1}\boldsymbol{\delta}\boldsymbol{\omega}\right) + \mathbf{d}(t) + \mathbf{u}, \tag{8a}$$

$$\dot{\boldsymbol{\eta}} = \boldsymbol{\psi} - \mathbf{M}^{-1}\boldsymbol{\delta}\boldsymbol{\omega}, \tag{8b}$$

$$\dot{\boldsymbol{\psi}} = -\left(\mathbf{C}\boldsymbol{\psi} + \mathbf{K}\boldsymbol{\eta} - \mathbf{C}\mathbf{M}^{-1}\boldsymbol{\delta}\boldsymbol{\omega}\right), \tag{8c}$$

where $\mathbf{J}_{mb} = \mathbf{J}_b - \boldsymbol{\delta}^{\mathrm{T}}\mathbf{M}^{-1}\boldsymbol{\delta} = \mathbf{J} + \Delta\mathbf{J}$ with $\Delta\mathbf{J}$ is the uncertain parameter matrix,

$$\mathbf{M} = \mu m_b \begin{bmatrix} 1 & 0 \\ 0 & 1 \end{bmatrix},$$
$$\mathbf{C} = \mathbf{M}^{-1}\begin{bmatrix} 2c_1 & 0 \\ 0 & 2c_2 \end{bmatrix}, \tag{9}$$
$$\mathbf{K} = m_p\mathbf{M}^{-1}\begin{bmatrix} g/l & 0 \\ 0 & g/l \end{bmatrix}.$$

If the terms $\Delta\mathbf{J}\dot{\boldsymbol{\omega}}$ and $\boldsymbol{\omega}^{\times}\Delta\mathbf{J}\boldsymbol{\omega}$ are the disturbances for the maneuver control system, equation (8a) can be rewritten as

$$\dot{\boldsymbol{\omega}} = \mathbf{J}^{-1}\left[-\boldsymbol{\omega}^{\times}\left(\mathbf{J}\boldsymbol{\omega} + \boldsymbol{\delta}^{\mathrm{T}}\boldsymbol{\psi}\right) + \boldsymbol{\delta}^{\mathrm{T}}\left(\mathbf{C}\boldsymbol{\psi} + \mathbf{K}\boldsymbol{\eta} - \mathbf{C}\mathbf{M}^{-1}\boldsymbol{\delta}\boldsymbol{\omega}\right) + \mathbf{T}_{\mathbf{d}} + \mathbf{u}\right], \tag{10}$$

where $\mathbf{T}_{\mathbf{d}} = -\Delta\mathbf{J}\dot{\boldsymbol{\omega}} - \boldsymbol{\omega}^{\times}\Delta\mathbf{J}\boldsymbol{\omega} + \mathbf{d}(t)$ is considered as the lumped disturbance.

All three components of the control torque $\mathbf{u}(t)$ are constrained by a priori fixed constant given by

$$\mathbf{u} \in \mathbf{S}_u = \{|u_i(t)| \le \bar{u}_m,\ i = 1, 2, 3\}, \tag{11}$$

where $\bar{u}_m$ is the largest amplitude of torque provided by the actuator.

2.3. Control Problem. In this work, the rest-to-rest attitude maneuver control problem is considered. The control aim is to achieve desired rotations for attitude $\mathbf{q}$ and angular velocity $\boldsymbol{\omega}$. The desired attitude and angular velocity are set to $\mathbf{q}_d = [0 \quad 0 \quad 0]^{\mathrm{T}}$ and $\boldsymbol{\omega}_d = [0 \quad 0 \quad 0]^{\mathrm{T}}$. The subsequent work is to design a robust saturated controller for maneuver control system (equation (10)) such that for any initial attitude quaternions and angular velocity

(1) all state variables in resulting closed-loop systems are uniformly bounded

(2) the controlled spacecraft achieves the objective that $\mathbf{q}(t)$ and $\boldsymbol{\omega}(t)$ will converge to the origin asymptotically under parametric uncertainty, external disturbances, and input saturation

3. Robust Adaptive Variable Structure Control Design

The primary objective of the VSC is to design a suitable algorithm for changing the structure of the control system during its operation [11, 14, 29]. Based on the existing results, an adaptive output feedback VSC is presented to achieve closed-loop stability with lumped disturbances and unknown input saturation.

3.1. Design of Sliding Mode Control for Spacecraft. The sliding surface in vector form is defined as follows:

$$\mathbf{s} = \boldsymbol{\omega} + k\mathbf{q}, \tag{12}$$

where k is a positive scalar. By multiplying both sides of equation (12) by $\mathbf{J}$, taking the derivative with respect to time, and using equations (8a), (8b), (8c), and (11), the following is obtained:

$$\mathbf{J}\dot{\mathbf{s}} = -\boldsymbol{\omega}^{\times}\mathbf{J}\boldsymbol{\omega} + \boldsymbol{\delta}^{\mathbf{T}}\left(\mathbf{C}\boldsymbol{\psi} + \mathbf{K}\boldsymbol{\eta} - \mathbf{C}\mathbf{M}^{-1}\boldsymbol{\delta}\boldsymbol{\omega}\right) + \mathbf{u} + \frac{1}{2}\mathbf{J}k(q_0\mathbf{I}_3 + \mathbf{q}^{\times})\boldsymbol{\omega}. \tag{13}$$

The form of control law is chosen as

$$\mathbf{u} = \mathbf{u}_{\mathrm{eq}} + \mathbf{u}_{\mathrm{vs}}, \tag{14}$$

where $\mathbf{u}_{\mathrm{eq}}$ represents the equivalent control component and the role of $\mathbf{u}_{\mathrm{eq}}$ is used to guarantee that $\dot{\mathbf{s}}(t) = 0$ for all time.

$$\mathbf{u}_{\mathrm{eq}} = \boldsymbol{\omega}^{\times}\mathbf{J}\boldsymbol{\omega} - \boldsymbol{\delta}^{\mathrm{T}}\left(\mathbf{C}\boldsymbol{\psi} + \mathbf{K}\boldsymbol{\eta} - \mathbf{C}\mathbf{M}^{-1}\boldsymbol{\delta}\boldsymbol{\omega}\right) - \frac{1}{2}\mathbf{J}k(q_0\mathbf{I}_3 + \mathbf{q}^{\times})\boldsymbol{\omega}. \tag{15}$$

Note that the control law (equation (14)) also includes the variable structure component; this component is selected to ensure that the sliding surface $\mathbf{s}(t) = 0$ as $t \to \infty$ can obtained in finite time. Its design is as follows:

$$V = \frac{1}{2}\mathbf{s}^{\mathrm{T}}\mathbf{J}\mathbf{s}. \tag{16}$$

The first derivative of V along the trajectory of the system can be obtained

$$\dot{V} = \mathbf{s}^{\mathrm{T}}\mathbf{u}_{\mathrm{vs}}, \tag{17}$$

by choosing

$$\mathbf{u}_{\mathrm{vs}} = -\sum(\mathbf{s})\boldsymbol{\alpha}, \tag{18}$$

where $\boldsymbol{\alpha} = [\alpha_1 \quad \alpha_2 \quad \alpha_3]^T$ with $\boldsymbol{\alpha}_i > 0$, $\sum(\mathbf{s}) = \mathrm{diag}\,[\mathrm{sgn}\,(s_1)\ \mathrm{sgn}\,(s_2)\mathrm{sgn}\,(s_3)]$. Here, sgn $(\cdot)$ denotes sign function and is defined as

$$\operatorname{sgn}(\beta) = \begin{cases} 1, & \beta > 0, \\ 0, & \beta = 0, \\ -1, & \beta < 0. \end{cases} \tag{19}$$

Substituting equation (18) into equation (17)

$$\dot{V} = -\mathbf{s}^{\mathrm{T}} \sum(\mathbf{s})\boldsymbol{\alpha} = -\sum_{i=1}^{3} \boldsymbol{\alpha}|\mathbf{s}_i| < 0. \tag{20}$$

It follows that $\mathbf{s} \in \mathbf{L}_\infty$ and $\lim_{t\to\infty} \mathbf{s} = 0$.

Remark 1. One of the main problems associated with the above-mentioned control law (equation (18)) is input chattering. This is induced by the imperfection of existing switching devices, namely, the sign function. Therefore, sign functions are usually replaced by saturation functions or approximate sign functions. It is important to note that the formulation in this paper uses the continuous hyperbolic tangent function instead of the typical switching function of variable structure control. As such, $\mathbf{u}_{\mathrm{vs}} = -\sum(\mathbf{s})\boldsymbol{\alpha}$ becomes $\bar{\mathbf{u}}_{\mathrm{vs}} = -\tanh(\mathbf{s})\boldsymbol{\alpha}$ and $\tanh(\mathbf{s})$ is expressed as

$$\tanh(\mathbf{s}) = [\tanh s_1 \quad \tanh s_2 \quad \tanh s_3]^{\mathrm{T}}. \tag{21}$$

Consider the same Lyapunov function (equation (18)), this yields

$$\dot{V} = \mathbf{s}^{\mathrm{T}} \bar{\mathbf{u}}_{\mathrm{vs}} \le -\|\boldsymbol{\alpha}\| \mathbf{s}^{\mathrm{T}} \tanh(\mathbf{s}) \le 0. \tag{22}$$

By using the fact that $\mathbf{s}^{\mathrm{T}} \tanh(\mathbf{s})$ is a positive-definite function in $\mathbf{s} \in R^3$, it is shown that $\lim_{t\to\infty} \mathbf{s} = 0$.

To determine the dynamics of spacecraft on the sliding surface, similar methods are adopted as in [11]. Once $\mathbf{s}(t) = 0$ is reached, the motion system will remain on the sliding surface. Therefore, the dynamics of spacecraft on the sliding surface can be obtained by using $\mathbf{s}(t) = 0$ to replace $\boldsymbol{\omega}$, namely, using equation (12) to substitute equation (7). This yields

$$\dot{q}_0 = -\frac{1}{2}\mathbf{q}^{\mathrm{T}}(-k\mathbf{q}) = \frac{k}{2}\left(1 - q_0^{\,2}\right), \tag{23}$$

$$\dot{\mathbf{q}} = \frac{1}{2}(q_0\mathbf{I} + \mathbf{q}^{\times})(-k\mathbf{q}) = -\frac{1}{2}kq_0\mathbf{q}. \tag{24}$$

The definition of t_f is the instant of time when the sliding mode $\mathbf{s} = 0$ is reached, and the following result is easily obtained by integrating the two sides of equation (23).

$$q_0(t) = 1 - \frac{2\left(1 - q_0(t_f)\right)e^{-k(t-t_f)}}{1 + q_0(t_f) + \left(1 - q_0(t_f)\right)e^{-k(t-t_f)}}, \quad t \ge t_f. \tag{25}$$

So $\lim_{t\to\infty} q_0 = 1$. Since the constraint relation of quaternions $q_0^{\,2} + \mathbf{q}^T\mathbf{q} = 1$ and the condition of reaching the sliding surface $\boldsymbol{\omega} = -k\mathbf{q}$, it can be concluded that $\lim_{t\to\infty} \|\mathbf{q}\| = \lim_{t\to\infty} \|\boldsymbol{\omega}\| = 0$.

Remark 2. Another problem associated with the preceding control law is caused by the quaternion direction representation. It is well known that $q_0 = 1$ and $q_0 = -1$ represent the same orientation. Since the above control method guarantees that the attitude of the spacecraft can be stabilized at $q_0 = 1$, namely, $\lim_{t\to\infty} q_0 = 1$, this shows that even if the initial position of the spacecraft is located very close to $q_0 = -1$, the spacecraft will rotate completely to derive point $q_0 = 1$. It should be mentioned that the aforementioned case is not an energy-efficient control scheme. To avoid this "unwinding phenomenon" described in [30], the sliding surface is modified to $\mathbf{s} = \boldsymbol{\omega} + k\mathbf{q}\operatorname{sgn}(q_0)$. Then, it is shown that

$$\dot{q}_0 = \frac{1}{2}\mathbf{q}^{\mathrm{T}}k\mathbf{q}\operatorname{sgn}(q_0) = \frac{k}{2}\left(1 - q_0^{\,2}\right)\operatorname{sgn}(q_0). \tag{26}$$

Equation (26) means that when the initial condition is $q(0) > 1$, the system reaches $\lim_{t\to 0} q_0 = 1$. Conversely, when the initial condition is $q(0) < 1$, the system reaches $\lim_{t\to 0} q_0 = -1$.

Remark 3. Another important problem related to the preceding control law is that it does not explicitly consider control input saturation. In addition, it is worth noting that disturbances always exist in the maneuver control system; however, the above control laws also do not take into account the rejection of disturbances.

An adaptive robust saturated control algorithm is proposed here to solve the above problem for liquid-filled spacecraft attitude maneuver. The proposed control scheme maintains the favorable characteristic of sliding mode control and uses the available control authority to achieve control objectives. This will be discussed in the following sections.

3.2. State Feedback Variable Structure Control Design with Time-Varying Sliding Surface. In order to give a clear design process of the control scheme, it is assumed that $\mathbf{T}_d = 0$ in this section. First, consider a simple control law can stabilize the control objective $\boldsymbol{\omega}$. Assuming that variables $\boldsymbol{\omega}$, $\mathbf{q}$, $\boldsymbol{\eta}$, and $\boldsymbol{\psi}$ are measurements available for feedback, given the Lyapunov function $V_2 = (1/2)\boldsymbol{\omega}^{\mathrm{T}}\mathbf{J}\boldsymbol{\omega}$, its first derivative with respect to time is obtained as follows:

$$\dot{V}_2 = \boldsymbol{\omega}^{\mathrm{T}}\left[\boldsymbol{\delta}^{\mathrm{T}}\begin{bmatrix}\mathbf{K}\\ \mathbf{C}\end{bmatrix}^{\mathrm{T}}\begin{bmatrix}\boldsymbol{\eta}\\ \boldsymbol{\psi}\end{bmatrix} - \boldsymbol{\delta}^{\mathrm{T}}\mathbf{C}\mathbf{M}^{-1}\boldsymbol{\delta}\boldsymbol{\omega} + \mathbf{u}\right]. \tag{27}$$

The form of the state feedback variable structure control is chosen to be

$$\mathbf{u} = -\boldsymbol{\delta}^{\mathrm{T}} \begin{bmatrix} \mathbf{K} \\ \mathbf{C} \end{bmatrix}^{\mathrm{T}} \begin{bmatrix} \boldsymbol{\eta} \\ \boldsymbol{\psi} \end{bmatrix} - k_d \tanh(\boldsymbol{\omega}), \tag{28}$$

where k_d is a positive constant. Substituting equation (28) into equation (27) yields

$$\begin{aligned} \dot{V}_2 &= -\boldsymbol{\omega}^{\mathrm{T}}\boldsymbol{\delta}^{\mathrm{T}}\mathbf{C}\mathbf{M}^{-1}\boldsymbol{\delta}\boldsymbol{\omega} - k_d\boldsymbol{\omega}^{\mathrm{T}}\tanh(\boldsymbol{\omega}) \le -\boldsymbol{\delta}^{\mathrm{T}}\mathbf{C}\mathbf{M}^{-1}\boldsymbol{\delta}\|\boldsymbol{\omega}\|^2 \\ &\quad - k_d\boldsymbol{\omega}^{\mathrm{T}}\tanh(\boldsymbol{\omega}) \le 0. \end{aligned} \tag{29}$$

By using Lyapunov's second method, it can be concluded that $\lim_{t\to\infty}\boldsymbol{\omega}(t) = 0$.

It is worth mentioning that the main goal is to stabilize $\boldsymbol{\omega}(t)$ and $\mathbf{q}(t)$; the question that arises in this case is whether a control law similar to equation (28) can be found to achieve this objective. In the analysis of the previous section, the equivalent control based on sliding control is designed. When the sliding surface $\mathbf{s} = 0$, it is obtained $\lim_{t\to\infty}\boldsymbol{\omega}(t) = \lim_{t\to\infty}\mathbf{q}(t) = 0$. Therefore, a control law is proposed, which can be composed of proportional attitude feedback term and augmented variable structure component. The state feedback variable structure control law can be obtained in the following form:

$$\begin{aligned} \mathbf{u} &= -k_p\mathbf{q} - \boldsymbol{\delta}^{T} \begin{bmatrix} \mathbf{K} \\ \mathbf{C} \end{bmatrix}^{\mathrm{T}} \begin{bmatrix} \boldsymbol{\eta} \\ \boldsymbol{\psi} \end{bmatrix} - k_d \tanh(\mathbf{s}) \\ &\quad - \frac{k_z}{2}(q_0\mathbf{I}_3 + \mathbf{q}^{\times})\tanh\left(\mathbf{q} - k_1{}^2\mathbf{z}\right), \end{aligned} \tag{30}$$

where k_p, k_z are positive constants; $\mathbf{z}(t) \in R^3$ is filter vector, and it can be calculated by the solution of linear differential equation $\dot{\mathbf{z}}(t) = \mathbf{q}(t) - k_1{}^2\mathbf{z}$.

Remark 4. The filter state $\mathbf{z}(t)$ satisfies the stable first-order linear vector differential equation and is forced by attitude vector $\mathbf{q}(t)$. In terms of frequency response characteristics, this filter dynamics can be considered as low-pass systems for all bounded $\mathbf{q}(t)$ signals. Also, it should be noted that the value of the filter gain k_1 plays a significant role in defining the low-pass characteristics of the filter state $\mathbf{z}(t)$. The choice of this design parameter depends on the level of signal noise encountered in the practical application [31].

Theorem 1. *For spacecraft attitude maneuver control systems governed by equations (7) and (10), the designed control law given in equation (30) can guarantee the global asymptotic stability of the closed-loop system.*

Proof. Consider the following Lyapunov function conditions

$$\begin{aligned} V_3 &= \frac{1}{2}\boldsymbol{\omega}^{\mathrm{T}}\mathbf{J}\boldsymbol{\omega} + k_p\left[\mathbf{q}^{\mathrm{T}}\mathbf{q} + (1-q_0)^2\right] \\ &\quad + k_z\sum_{i=1}^{3}\log\cosh\left(\mathbf{q}_i - k_1{}^2\mathbf{z}_i\right) + \frac{1}{2\gamma}k^2 \\ &= \frac{1}{2}\boldsymbol{\omega}^{\mathrm{T}}\mathbf{J}\boldsymbol{\omega} + 2k_p(1-q_0) \\ &\quad + k_z\sum_{i=1}^{3}\log\cosh\left(\mathbf{q}_i - k_1{}^2\mathbf{z}_i\right) + \frac{1}{2\gamma}k^2, \end{aligned} \tag{31}$$

where parameter $k(t)$ is a time-varying function and an adaptive updating law is designed for $k(t)$ subsequently.

The first derivative of equation (31) is given by

$$\begin{aligned} \dot{V}_3 &= \boldsymbol{\omega}^{\mathrm{T}}\mathbf{J}\dot{\boldsymbol{\omega}} - 2k_p\dot{q}_0 - k_z\left[\dot{\mathbf{q}} - k_1{}^2\dot{\mathbf{z}}\right]^{\mathrm{T}}\tanh\left(\mathbf{q} - k_1{}^2\mathbf{z}\right) + \frac{1}{\gamma}k\dot{k} \\ &= \boldsymbol{\omega}^{\mathrm{T}}\Big\{-\boldsymbol{\omega}^{\times}\left(\mathbf{J}\boldsymbol{\omega} + \boldsymbol{\delta}^{\mathrm{T}}\boldsymbol{\psi}\right) + \boldsymbol{\delta}^{\mathrm{T}}\left(\mathbf{C}\boldsymbol{\psi} + \mathbf{K}\boldsymbol{\eta} - \mathbf{C}\mathbf{M}^{-1}\boldsymbol{\delta}\boldsymbol{\omega}\right) \\ &\quad - k_p\mathbf{q} - \boldsymbol{\delta}^{\mathrm{T}}\begin{bmatrix} \mathbf{K} \\ \mathbf{C} \end{bmatrix}^{\mathrm{T}}\begin{bmatrix} \boldsymbol{\eta} \\ \boldsymbol{\psi} \end{bmatrix} - k_d\tanh(\mathbf{s}) \\ &\quad - k_z/2(q_0\mathbf{I}_3 + \mathbf{q}^{\times})\tanh\left(\mathbf{q} - k_1{}^2\mathbf{z}\right)\Big\} \\ &\quad - 2k_p\dot{q}_0 + k_z\left[\dot{\mathbf{q}} - k_1{}^2\dot{\mathbf{z}}\right]^{\mathrm{T}}\tanh\left(\mathbf{q} - k_1{}^2\mathbf{z}\right) + \frac{1}{\gamma}k\dot{k} \\ &= -\boldsymbol{\omega}^{\mathrm{T}}\boldsymbol{\delta}^{\mathrm{T}}\mathbf{C}\mathbf{M}^{-1}\boldsymbol{\delta}\boldsymbol{\omega} - k_zk_1{}^2(\dot{\mathbf{z}})^{\mathrm{T}}\tanh(\dot{\mathbf{z}}) - k_d\boldsymbol{\omega}^{\mathrm{T}}\tanh(\mathbf{s}) + \frac{1}{\gamma}k\dot{k}. \end{aligned} \tag{32}$$

The updating law for k is designed to satisfy

$$\dot{k} = -\gamma k_d\mathbf{q}^{\mathrm{T}}\tanh(\mathbf{s}), \tag{33}$$

where γ is a positive constant.

According to equation (32), equation (33) can be rewritten as

$$\dot{V}_3 = -\boldsymbol{\omega}^{\mathrm{T}}\boldsymbol{\delta}^{\mathrm{T}}\mathbf{C}\mathbf{M}^{-1}\boldsymbol{\delta}\boldsymbol{\omega} - k_zk_1{}^2(\dot{\mathbf{z}})^{\mathrm{T}}\tanh(\dot{\mathbf{z}}) - k_d\mathbf{s}^{\mathrm{T}}\tanh(\mathbf{s}) \le 0. \tag{34}$$

The integral on both sides of equation (34) yields $\sup_{t\ge 0} V(t) \le V(0)$. This shows that $V_3(t)$ is a bounded function, such that $\boldsymbol{\omega}$, $\mathbf{q}$, $\mathbf{z}(t)$, $\dot{\mathbf{z}}(t)$ is uniformly bounded. Due to the boundedness of all signals in the time derivative of equation (34), it is easy to demonstrate that $\ddot{V}_3(t)$ is bounded, and the uniform continuity of $\dot{V}_3(t)$ can be obtained. Applying the Barbalat lemma to obtain $\dot{V}(t) \to 0$ as $t \to \infty$which further leads to the conclusion that $\lim_{t\to\infty}\boldsymbol{\omega} = \lim_{t\to\infty}\mathbf{s} = 0$, and from this result, it can be concluded that $\lim_{t\to\infty}k\mathbf{q} = 0$. Next, since the third derivative of $\mathbf{z}(t)$ function for time is uniformly bounded, this proves that $\ddot{\mathbf{z}}(t)$is uniformly bounded.

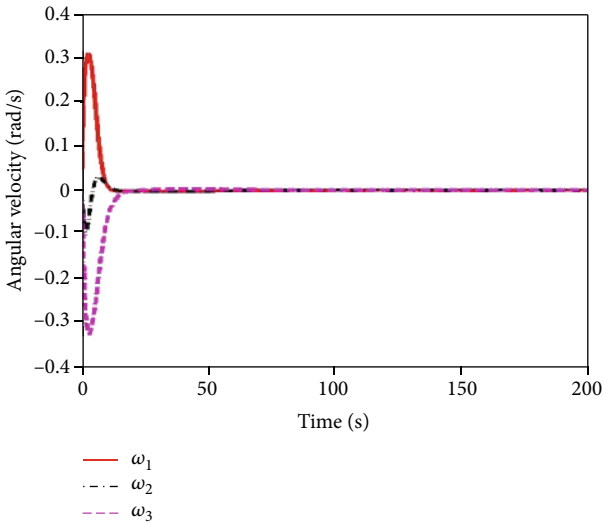

Figure 2: Time histories of angular velocities in Case 1.

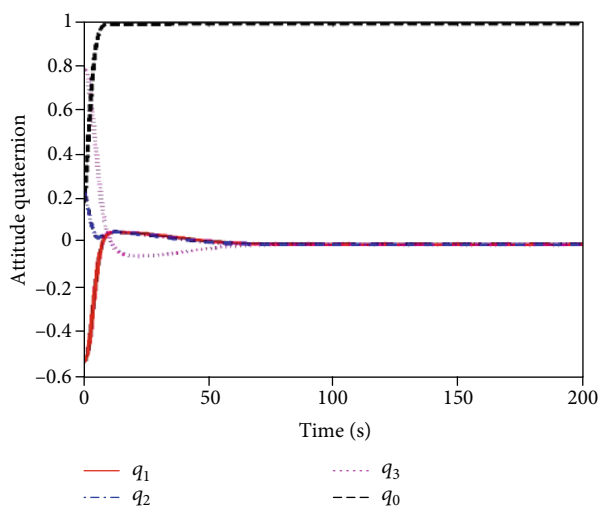

Figure 3: Time histories of attitude quaternions in Case 1.

Additionally, since $\lim_{t\to\infty}\dot{\mathbf{z}}(t)=0$, the following results are obtained:

$$\lim_{t\to\infty}\int_0^t \ddot{\mathbf{z}}(\tau)d\tau=\lim_{t\to\infty}\dot{\mathbf{z}}(t)=0. \tag{35}$$

Using Barbalat's lemma, it is shown that $\lim_{t\to\infty}\ddot{\mathbf{z}}(t)=0$; since $\ddot{\mathbf{z}}(t)=\dot{\mathbf{q}}-k^2\dot{\mathbf{z}}(t)$, it follows that $\lim_{t\to\infty}\dot{\mathbf{q}}=0$ as $t\to\infty$. According to the above obtained conclusion and the boundness of signals on the right side of equation (7), it can verify that $\ddot{\mathbf{q}}(t)$ is uniformly bounded; hence, applying the uniform continuity for $\lim_{t\to\infty}\dot{\mathbf{q}}=0$, the following results are obtained:

$$\lim_{t\to\infty}\int_0^t \dot{\mathbf{q}}(\tau)\mathrm{d}\tau=\lim_{t\to\infty}\mathbf{q}(t)=0, \tag{36}$$

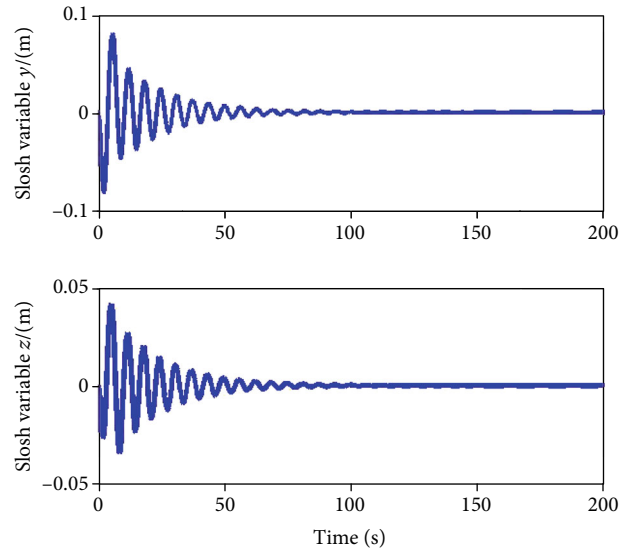

Figure 4: Time histories of liquid sloshing displacement in Case 1.

and reusing Barbalat's lemma, the result $\lim_{t\to\infty}\mathbf{q}=0$ is obtained. Because $\lim_{t\to\infty}\boldsymbol{\omega}=0$, using equations (8a), (8b), and (8c), one can conclude that $\ddot{\boldsymbol{\omega}}(t)$ is bounded. This means that $\dot{\boldsymbol{\omega}}(t)$ is uniformly bounded. By implying Barbalat's lemma, it is possible to conclude that $\lim_{t\to\infty}\dot{\boldsymbol{\omega}}=0$. Further, note that $\mathbf{J}\dot{\boldsymbol{\omega}}\to 0$ as $t\to\infty$ such that $[\boldsymbol{\eta}\quad\boldsymbol{\psi}]^{\mathrm{T}}\to 0$ as $t\to\infty$. Thus, the trajectory of the system converges to

$$\lim_{t\to\infty}\left((t),\mathbf{s}(t),\begin{bmatrix}\boldsymbol{\eta}\\ \boldsymbol{\psi}\end{bmatrix}\right)=0. \tag{37}$$

Remark 6. The state feedback control law requires all states to be measurable. This is a very difficult condition to achieve in practical application. In addition, the value of k also affects the system response since k is used to achieve the relative weight between $\boldsymbol{\omega}(t)$ and $\mathbf{q}(t)$. A smaller k will result in a slow response in $\mathbf{q}(t)$. Also, it is worth mentioning that the control law (equation (30)) does not consider the rejection of disturbance and the control input saturation. In this case, adaptive output feedback control strategy is used to solve this kind of problem.

3.3. Adaptive Output Feedback Variable Structure Control under Actuator Saturation

3.3.1. Radial Basis Function Neural Network (RBFNN). Due to the universal approximation characteristics and learning ability of neural networks (NN), NN have proven to be a powerful tool for controlling complex dynamic nonlinear systems with parametric uncertainties. Due to its simple structure and good approximation ability, RBFNN is employed to approximate the continuous function in the present work. First, the input of the saturated nonlinear control is approximated by a smooth function defined as [27]

$$\mathbf{v}=\mathbf{g}(\mathbf{u})=\mathbf{u}+\Delta\mathbf{u}, \tag{38}$$

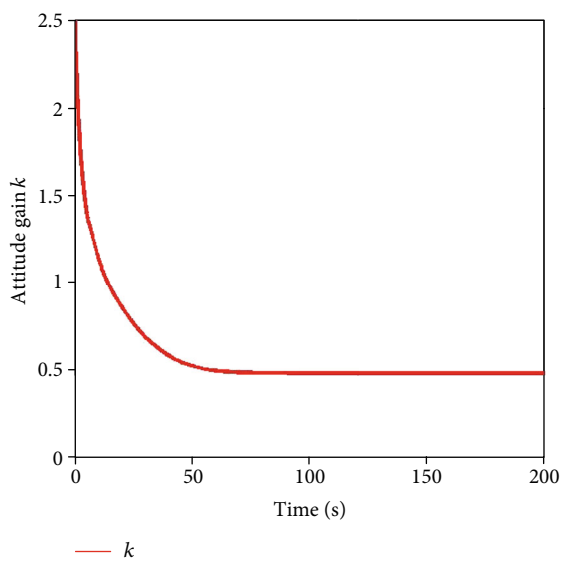

Figure 5: Time histories of attitude gain k in Case 1.

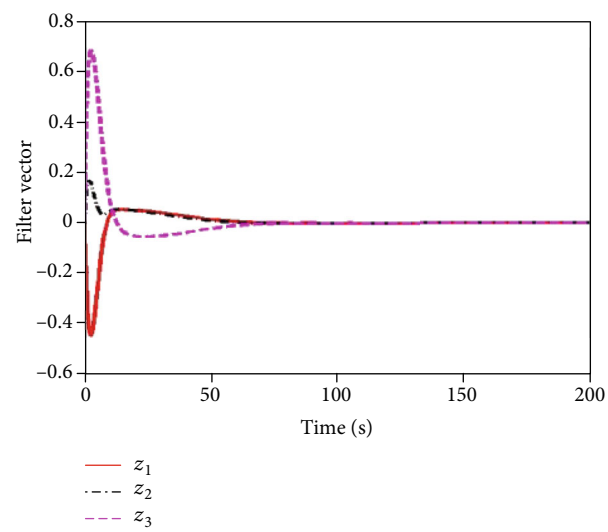

Figure 6: Time histories of filter vector in Case 1.

where $\mathbf{v} = [v_1 \quad v_2 \quad v_3]^{\mathrm{T}}$ represents the control torque to be designed and $\mathbf{g}(\mathbf{u})$ is defined as

$$\mathbf{g}(\mathbf{u}) = u_{\max} \times \tanh\left(\frac{\mathbf{u}}{u_{\max}}\right). \tag{39}$$

Assuming that $\Delta\mathbf{u}$ is unknown and from the perspective of compensation, the saturated component can be considered as a system disturbance and compensated by feed-forward scheme. Since $\Delta\mathbf{u} = \mathbf{g}(\mathbf{u}) - \mathbf{u}$ is a continuous function that can be approximated by a radial basis function neural network (RBFNN), it is well known that as long as the NN is large enough, the neural network can approximate any continuous function with arbitrary precision. For a continuous nonlinear function $f(\mathbf{x}) \in \mathbf{R}$, it can be approximated as

$$\begin{aligned} f(\mathbf{x}) &= \widehat{f}(\mathbf{x}, \boldsymbol{\theta}^*) + \boldsymbol{\varepsilon} = \boldsymbol{\theta}^{*\mathrm{T}}\phi(\mathbf{x}) + \boldsymbol{\varepsilon}, \\ \varphi_n &= \exp\left(-\frac{\|\mathbf{x} - \mathbf{c}_i\|^2}{\sigma_i^2}\right), \quad i = 1, 2, \cdots, n, \end{aligned} \tag{40}$$

where $\mathbf{x} \in R^n$ and $\boldsymbol{\varepsilon} \in R$ represent the input signals of the neural network and approximation error, respectively.

And $\phi(\mathbf{x}) = [\varphi_1(x), \varphi_2(x), \varphi_3(x), \cdots, \varphi_l(x)]^T \in \mathbf{R}^l$ is a known continuous smooth vector value function; $\varphi_i(\mathbf{x})$ are selected as the commonly used Gaussian function. l is called the number of neural network nodes. $\boldsymbol{\theta}^* \in \mathbf{R}^n$ is the optimal weight vector, and $\mathbf{c}_i \in \mathbf{R}^n$ and $\sigma_{\mathrm{i}} > 0$ are the center vector and radial basis vector of $\phi(\mathbf{x})$, respectively. The RBFNN output $\widehat{f}(\mathbf{x}, \boldsymbol{\theta}^*)$ is the approximation value of $f(\mathbf{x})$. Optimal weight vector is defined as

$$\boldsymbol{\theta}^* = [\theta_1{}^*(x), \theta_2{}^*(x), \theta_3{}^*(x), \cdots, \theta_l{}^*(x)] \in \mathbf{R}^l. \tag{41}$$

In general, $\boldsymbol{\theta}^*$ is the vector selected from $\boldsymbol{\theta}$ to minimize $\|f(\mathbf{x}) - \widehat{f}(\mathbf{x}, \boldsymbol{\theta})\|$. Mathematically, that is

$$\boldsymbol{\theta}^* = \arg \min_{\widehat{\boldsymbol{\theta}}} \left\{ \sup_{\mathbf{x} \in \Omega} \left\| f(x) - \widehat{f}(\mathbf{x}, \boldsymbol{\theta}) \right\| \right\}, \tag{42}$$

where $\widehat{\boldsymbol{\theta}}$ is the estimation value of $\boldsymbol{\theta}^*$, $\Omega \in R^l$ is compact set.

For MIMO systems, the nonlinear function $\Delta\mathbf{u}$ can be approximated using the RBF network as follows:

$$\Delta\mathbf{u} = \boldsymbol{\theta}^{*T}\phi(\mathbf{x}) + \boldsymbol{\varepsilon}, \tag{43}$$

where $\mathbf{x} = [\mathbf{q}^{\mathrm{T}} \quad \boldsymbol{\omega}^{\mathrm{T}}]^{\mathrm{T}}$ and $\boldsymbol{\theta}^* \in R^{l\times 3}$, $\boldsymbol{\theta}^* = [\boldsymbol{\theta}_1{}^{*\mathrm{T}}(\mathbf{x}), \ \boldsymbol{\theta}_2{}^{*\mathrm{T}}(\mathbf{x}), \boldsymbol{\theta}_3{}^{*T}(\mathbf{x})]^{\mathrm{T}}$, $\boldsymbol{\varepsilon} = [\varepsilon_1 \quad \varepsilon_2 \quad \varepsilon_3]^{\mathrm{T}}$.

Assumption 7. According to the universal approximation property of RBF network, the maximum mean square value of approximation error vector is bounded and satisfies $\|\boldsymbol{\varepsilon}\| \le \varepsilon_0$, in which ε_0 is a small constant.

Assumption 8. The ideal NN optimal weight $\boldsymbol{\theta}^*$ is bounded, such that $\|\boldsymbol{\theta}^*\| \le \theta_m$ and θ_m is a positive constant.

3.3.2. Adaptive Output Feedback Variable Structure Control with RBFNN-Based Saturation Scheme. To remove the drawbacks discussed in Remark 11 for the control law (equation (30)), the derived controller in the previous section is extended to the output feedback case to estimate attitude gain function $k(t)$ and the liquid sloshing displacement variable by selecting the appropriate adaptive control law. Simultaneously, compensation scheme-based neural network is implemented as feed-forward control method to compensate nonlinear saturation effects.

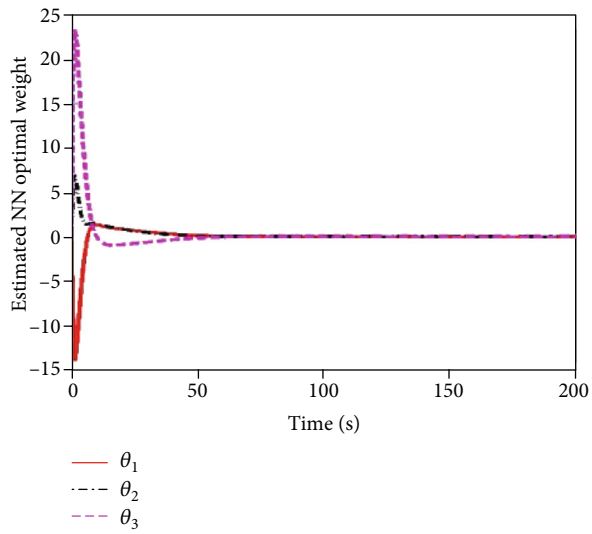

Figure 7: Time histories of estimated NN optimal weight in Case 1.

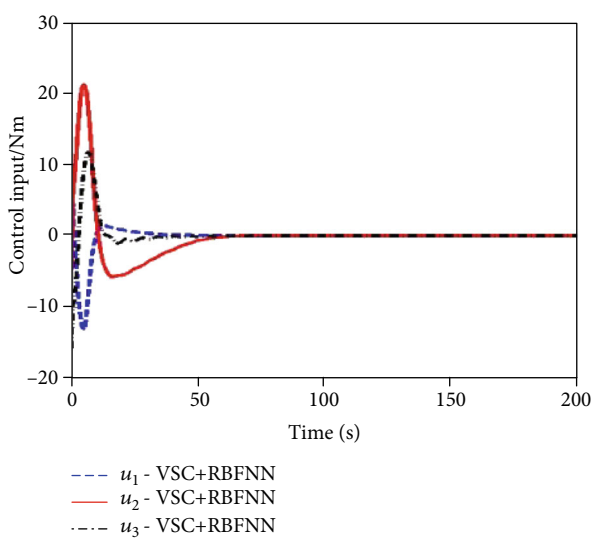

Figure 8: Time histories of control input in Case 1.

The adaptive output feedback VSC is proposed as follows:

$$\mathbf{u}(t) = -k_p\mathbf{q} - \boldsymbol{\delta}^{\mathrm{T}}\begin{bmatrix}\mathbf{K}\\ \mathbf{C}\end{bmatrix}^{\mathrm{T}}\begin{bmatrix}\widehat{\boldsymbol{\eta}}\\ \widehat{\boldsymbol{\psi}}\end{bmatrix} - k_d \tanh(\mathbf{s}) - \frac{k_z}{2}(q_0\mathbf{I}_3 + \mathbf{q}^{\times})\tanh\left(\mathbf{q} - k_1{}^2\mathbf{z}\right) - \boldsymbol{\theta}\wedge^{\mathrm{T}}\phi(\mathbf{x}). \tag{44a}$$

Modified updating law for k is designed to satisfy

$$\dot{k} = -\frac{\gamma}{k}\left[k_q k\mathbf{q}^{\mathrm{T}}\tanh(\mathbf{s}) + \sum_{i=1}^{3}\left(L_i s_i \operatorname{sgn}(k) + L_i k q_i \operatorname{sgn}(s_i)\right)\right]. \tag{44b}$$

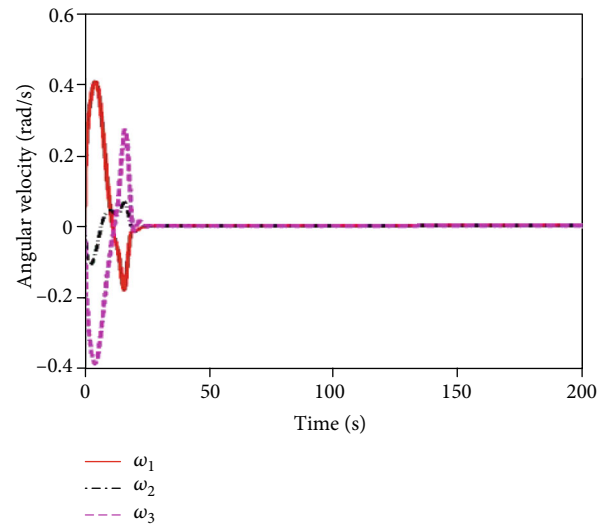

Figure 9: Time histories of angular velocities in Case 2.

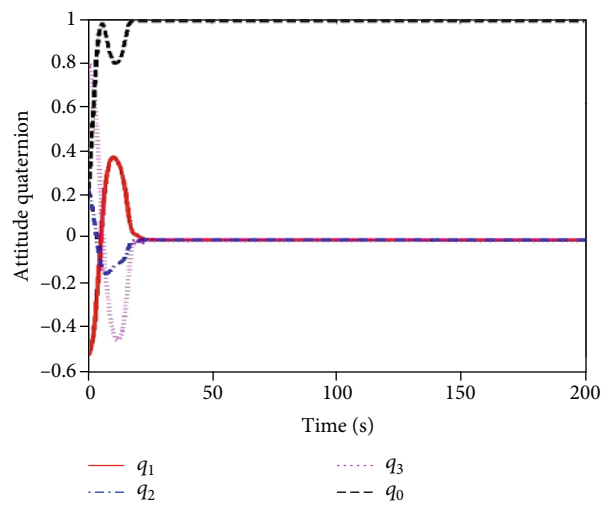

Figure 10: Time histories of attitude quaternions in Case 2.

Adaptive updating law for liquid sloshing displacement variable is designed as

$$\begin{bmatrix}\dot{\widehat{\boldsymbol{\eta}}}\\ \dot{\widehat{\boldsymbol{\psi}}}\end{bmatrix} = \mathbf{A}\begin{bmatrix}\widehat{\boldsymbol{\eta}}\\ \widehat{\boldsymbol{\psi}}\end{bmatrix} - \begin{bmatrix}\mathbf{I}\\ -\mathbf{C}\end{bmatrix}\mathbf{M}^{-1}\boldsymbol{\delta}\boldsymbol{\omega} - \boldsymbol{\Gamma}^{-1}\begin{bmatrix}\mathbf{K}\\ \mathbf{C}\end{bmatrix}\boldsymbol{\delta}\boldsymbol{\omega}. \tag{44c}$$

Neural network compensator updating law is given by

$$\dot{\widehat{\boldsymbol{\theta}}} = \mathbf{P}\left(\phi(\mathbf{x})\boldsymbol{\omega}^{\mathrm{T}} - \delta_\theta\|\mathbf{s}\|\widehat{\boldsymbol{\theta}}\right), \tag{44d}$$

where

$$\mathbf{A} = \begin{bmatrix}\mathbf{0} & \mathbf{I}\\ -\mathbf{K} & -\mathbf{C}\end{bmatrix}. \tag{45}$$

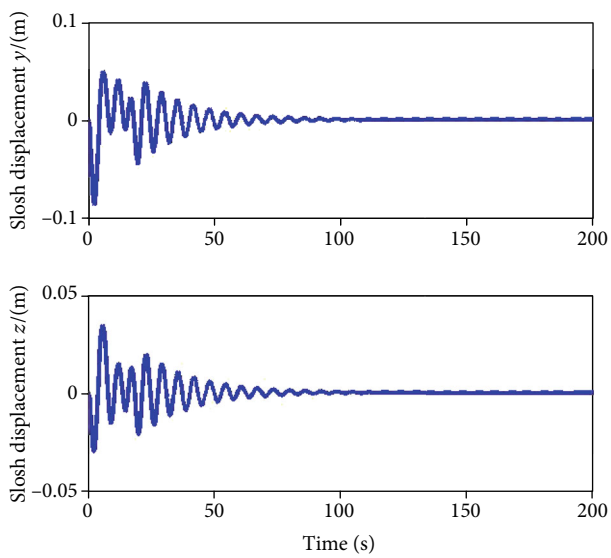

Figure 11: Time histories of liquid sloshing displacement in Case 2.

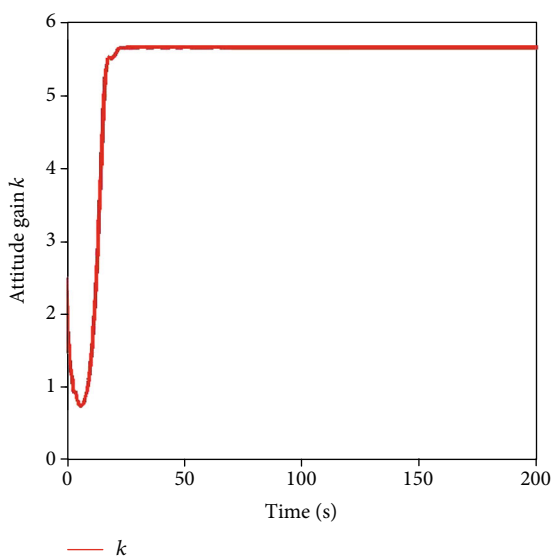

Figure 12: Time histories of attitude gain $k(t)$ in Case 2.

$\mathbf{\Gamma} \in \mathbf{R}^{4\times 4}$ and $\mathbf{P} \in \mathbf{R}^{l\times l}$ are positive definite symmetric matrices. $\gamma > 0$ denotes an adaptive attitude gain.

Assumption 9. It is assumed that the positive constant L_i strictly dominates the unknown disturbance $\mathbf{T}_d$ and small constant ε_0, namely, $\|\mathbf{T}_{di}\| \le d_m \le d_m + \varepsilon_0 + 1/2\delta_\theta \theta_m{}^2 \le L_i$ is satisfied, $\forall T \ge 0$, $i = 1, 2, 3$, where δ_θ is a small positive constant.

Theorem 2. *Consider the attitude maneuver control system governed by equations (7) and (10), if control input $\mathbf{u}(t)$ is given by equation (44a) with the adaptive control law given by equations (44b) and (44c) and NN compensator updating law given by equation (44d). All trajectories of the closed-loop system obtained are uniformly bounded for all $t \ge 0$. In addition, they asymptotically converge to the set defined by $\lim_{t\to\infty} (\mathbf{s}(t), \mathbf{z}(t), [\mathbf{e}_\eta \quad \mathbf{e}_\psi], \widetilde{\boldsymbol{\theta}}) = 0$.*

Proof. Consider the following Lyapunov function candidate:

$$V_4 = \frac{1}{2}\boldsymbol{\omega}^{\mathrm{T}}\mathbf{J}\boldsymbol{\omega} + 2k_p(1-q_0) + \frac{1}{2}\begin{bmatrix}\mathbf{e}_\eta & \mathbf{e}_\psi\end{bmatrix}^{\mathrm{T}}\mathbf{\Gamma}\begin{bmatrix}\mathbf{e}_\eta \\ \mathbf{e}_\psi\end{bmatrix} + k_z\sum_{i=1}^{3}\log\cosh\left(q_i - k_1{}^2\mathbf{z}_i\right) + \frac{1}{2\gamma}k^2 + \frac{1}{2}\mathrm{tr}\left(\widetilde{\boldsymbol{\theta}}^{\mathrm{T}}\mathbf{P}^{-1}\widetilde{\boldsymbol{\theta}}\right), \tag{46}$$

where $\mathrm{tr}(\cdot)$ represents the trace of a matrix $(\cdot)$.

The first derivative with respect to time can be obtained by computing V_4 along the trajectory of the system

$$\begin{aligned}\dot{V}_4 = \boldsymbol{\omega}^{\mathrm{T}}\Bigg\{&-\boldsymbol{\omega}^{\times}\left(\mathbf{J}\boldsymbol{\omega} + \boldsymbol{\delta}^{\mathrm{T}}\boldsymbol{\psi}\right) + \boldsymbol{\delta}^{T}\begin{bmatrix}\mathbf{K}\\ \mathbf{C}\end{bmatrix}^{\mathrm{T}}\begin{bmatrix}\boldsymbol{\eta}\\ \boldsymbol{\psi}\end{bmatrix} - \boldsymbol{\delta}^{\mathrm{T}}\boldsymbol{C}\boldsymbol{M}^{-1}\boldsymbol{\delta}\boldsymbol{\omega} + \mathbf{d}(t)\\ &- k_p\mathbf{q} - \boldsymbol{\delta}^{\mathrm{T}}\begin{bmatrix}\mathbf{K}\\ \mathbf{C}\end{bmatrix}^{\mathrm{T}}\begin{bmatrix}\widehat{\boldsymbol{\eta}}\\ \widehat{\boldsymbol{\psi}}\end{bmatrix} - k_d\tanh(\mathbf{s})\\ &- k_z/2(q_0\mathbf{I}_3 + \mathbf{q}^{\times})\tanh\left(\mathbf{q} - k_1{}^2\mathbf{z}\right) + \widetilde{\boldsymbol{\theta}}^{\mathbf{T}}\phi(\mathbf{x}) + \boldsymbol{\varepsilon}\Bigg\}\\ &+ \begin{bmatrix}\mathbf{e}_\eta & \mathbf{e}_\psi\end{bmatrix}^{\mathrm{T}}\mathbf{\Gamma}\left(\mathbf{A}\begin{bmatrix}\boldsymbol{\eta}\\ \boldsymbol{\psi}\end{bmatrix} - \begin{bmatrix}\mathbf{I}\\ -\mathbf{C}\end{bmatrix}\mathbf{M}^{-1}\boldsymbol{\delta}\boldsymbol{\omega} - \begin{bmatrix}\dot{\widehat{\boldsymbol{\eta}}}\\ \dot{\widehat{\boldsymbol{\psi}}}\end{bmatrix}\right)\\ &+ k_z\left(\dot{\mathbf{q}} - k_1{}^2\dot{\mathbf{z}}\right)^{\mathrm{T}}\tanh\left(\mathbf{q} - k_1{}^2\mathbf{z}\right) + \frac{1}{\gamma}k\dot{k} + \mathrm{tr}\left(\widetilde{\boldsymbol{\theta}}^{\mathrm{T}}\mathbf{P}^{-1}\dot{\widetilde{\boldsymbol{\theta}}}\right)\\ \le &-\lambda_m\left(\boldsymbol{\delta}^{\mathrm{T}}\mathbf{C}\mathbf{M}^{-1}\boldsymbol{\delta}\right)\|\boldsymbol{\omega}\|^2 + \|\mathbf{s} - k\mathbf{q}\|(d_m + \varepsilon_0)\\ &- L_i\left(\sum_{i=1}^{3}s_i\,\mathrm{sgn}(k) + kq_i\,\mathrm{sgn}(s_i)\right)\\ &- k_q\mathbf{s}^{\mathrm{T}}\tanh(\mathbf{s}) - k_zk_1{}^2(\dot{\mathbf{z}})^{\mathrm{T}}\tanh(\dot{\mathbf{z}})\\ &- \begin{bmatrix}\mathbf{e}_\eta & \mathbf{e}_\psi\end{bmatrix}^{\mathrm{T}}\mathbf{Q}\begin{bmatrix}\mathbf{e}_\eta\\ \mathbf{e}_\psi\end{bmatrix} + \delta_\theta\mathrm{tr}\left[\widetilde{\boldsymbol{\theta}}^{\mathrm{T}}\mathbf{s}\left(\boldsymbol{\theta}^* - \widetilde{\boldsymbol{\theta}}\right)\right].\end{aligned} \tag{47}$$

It is worth mentioning that the following inequality holds:

$$\mathrm{tr}\left[\widetilde{\boldsymbol{\theta}}^{\mathrm{T}}\mathbf{s}\left(\boldsymbol{\theta}^* - \widetilde{\boldsymbol{\theta}}\right)\right] \le \|\mathbf{s}\|\left\|\widetilde{\boldsymbol{\theta}}\right\|\|\boldsymbol{\theta}^*\| - \|\mathbf{s}\|\left\|\widetilde{\boldsymbol{\theta}}\right\|^2 \le \frac{1}{2}\|\mathbf{s}\|\|\boldsymbol{\theta}^*\|^2 - \frac{1}{2}\|\mathbf{s}\|\left\|\widetilde{\boldsymbol{\theta}}\right\|^2. \tag{48}$$

Substituting equation (48) into equation (47), it can obtain

$$\begin{aligned}\dot{V}_4 \le & -\lambda_m\left(\boldsymbol{\delta}^{\mathrm{T}}\mathbf{C}\mathbf{M}^{-1}\boldsymbol{\delta}\right)\|\boldsymbol{\omega}\|^2 + \|\mathbf{s}-k\mathbf{q}\|(d_m+\varepsilon_0) \\ & - k_z k_1{}^2(\dot{\mathbf{z}})^{\mathrm{T}}\tanh(\dot{\mathbf{z}}) - k_q\mathbf{s}^{\mathrm{T}}\tanh(\mathbf{s}) - \begin{bmatrix}\mathbf{e}_\eta & \mathbf{e}_\psi\end{bmatrix}^{\mathrm{T}}\mathbf{Q}\begin{bmatrix}\mathbf{e}_\eta \\ \mathbf{e}_\psi\end{bmatrix} \\ & + \frac{1}{2}\delta_\theta\theta_m{}^2\|\mathbf{s}\| - \frac{1}{2}\delta_\theta\|\mathbf{s}\|\left\|\widetilde{\boldsymbol{\theta}}\right\|^2 - L_i\sum_{i=1}^{3}|s_i| - L_i\sum_{i=1}^{3}k|q_i| \\ \le & -\lambda_m\left(\boldsymbol{\delta}^{\mathrm{T}}\mathbf{C}\mathbf{M}^{-1}\boldsymbol{\delta}\right)\|\boldsymbol{\omega}\|^2 - k_z k_1{}^2(\dot{\mathbf{z}})^{\mathrm{T}}\tanh(\dot{\mathbf{z}}) \\ & - (L_i - d_m - \varepsilon_0)\sum_{i=1}^{3}(k|q_i(t)|) - \left(\|\mathbf{s}_1\| + L_i - d_m - \varepsilon_0 - \frac{1}{2}\delta_\theta\theta_m{}^2\right) \\ & \sum_{i=1}^{3}(|s_i|) - \begin{bmatrix}\mathbf{e}_\eta & \mathbf{e}_\psi\end{bmatrix}^{\mathrm{T}}\mathbf{Q}\begin{bmatrix}\mathbf{e}_\eta \\ \mathbf{e}_\psi\end{bmatrix} - \frac{1}{2}\delta_\theta\left\|\widetilde{\boldsymbol{\theta}}\right\|^2\sum_{i=1}^{3}(|s_i|)\end{aligned} \tag{49}$$

Note the fact that

$$\boldsymbol{\omega}^{\mathrm{T}}(\mathbf{T}_d + \boldsymbol{\varepsilon}) \le \|\boldsymbol{\omega}\|(d_m+\varepsilon_0) \le (d_m+\varepsilon_0)\left(\sum_{i=1}^{3}|s_i| + k|q_i|\right), \tag{50}$$

where $\mathbf{s}_1 = k_p\tanh(\mathbf{s})$ and $\lambda_m(\cdot)$ is the minimum eigenvalues of the matrix $(\cdot)$. $\boldsymbol{\Gamma}$ can be computed as the solution of $\boldsymbol{\Gamma}\mathbf{A} + \mathbf{A}\boldsymbol{\Gamma}^{\mathrm{T}} = -2\mathbf{Q}$ for any fixed $\mathbf{Q} = \mathbf{Q}^{\mathrm{T}} > 0$.

From Assumption 9, it is easy to show that

$$\dot{V}_4 \le 0. \tag{51}$$

It can be seen that $\boldsymbol{\omega}(t), \mathbf{q}(t), \mathbf{z}(t), \dot{\mathbf{z}}(t), \widetilde{\boldsymbol{\theta}}$, and $\begin{bmatrix}\mathbf{e}_\eta & \mathbf{e}_\psi\end{bmatrix}^{\mathrm{T}}$ are all uniformly bounded. It can also be concluded that $\ddot{V}(t)$ is bounded, which means that $\dot{V}(t)$ is uniform continuity function and $\lim_{t\to\infty}\dot{V}(t) = 0$ is obtained using Barbalat's lemma. Here, the analysis process is similar to the previous section by using Barbalat's lemma; thus, the following results are revealed:

$$\lim_{t\to\infty}\left\{k(t)\mathbf{q}(t) = 0, \mathbf{z}(t), \mathbf{s}(t) = 0, \begin{bmatrix}\mathbf{e}_\eta & \mathbf{e}_\psi\end{bmatrix}, \widetilde{\boldsymbol{\theta}}\right\} = 0.. \tag{52}$$

This completes the proof of Theorem 2.

Remark 11. According to the proof of Theorem 2, the adaptive output feedback control scheme developed in equation (46) can achieve the attitude stabilization maneuver of the liquid-filled spacecraft with lumped disturbances and input saturation.

Remark 12. It should be noted that Theorem 2 only guarantees that $k(t)\mathbf{q}(t) = 0$ as $t \to \infty$; this will not necessarily ensure that $\mathbf{q}(t)$ will converge to zero. If $k(t)$ converges to zero faster than $\mathbf{q}(t)$, then $\mathbf{q}(t)$ will converge to a nonzero constant value. In order to guarantee that $\mathbf{q}(t)$ converge to zero, it is necessary to prevent $k(t)$ from converging to zero. This can be achieved by using a sufficiently small γ to ensure $k(t)$ changes slowly such that it does not deviate too much from its initial value. In addition, since $k(t)$ is used to achieve relative weights between $\boldsymbol{\omega}(t)$ and $\mathbf{q}(t)$, a smaller $k(t)$ will result in slow response of $\mathbf{q}(t)$. Conversely, a higher $k(t)$ will lead to oscillatory response in system. Subsequent numerical simulation examples show that appropriate initial value $k(0)$ and/or small enough parameter γ can be found in most cases. This ensures that the sliding mode $\mathbf{s}$ converges to the origin under parametric uncertainty, external disturbances, and input saturation. In other words, initial value $k(0)$ and parameter γ need to be correctly selected to tune the controller within acceptable transient response and performance.

Remark 13. According to the definition of attitude quaternions in equations (8a), (8b), and (8c) and the property of hyperbolic tangent function, it can be easily obtained that $\|q_0\mathbf{I}_3 + \mathbf{q}^{\times}\| \le 1$, $\|\mathbf{q}\| \le 1$, and $\|\tanh(\mathbf{s} - k_1{}^2\mathbf{z})\| \le 1$. If the term

$$\boldsymbol{\delta}^T\begin{bmatrix}\mathbf{K} \\ \mathbf{C}\end{bmatrix}^{\mathrm{T}}\begin{bmatrix}\widehat{\boldsymbol{\eta}} \\ \widehat{\boldsymbol{\psi}}\end{bmatrix} \tag{53}$$

is not considered in equation (46), note that the control input satisfies the input saturation limitations, namely, $\|\mathbf{u}(t)\| \le k_p + k_q + k_z/2 \le \bar{u}_m$. This indicates that the RBFNN saturation compensator is used to compensate for saturation uncertainty caused by term

$$\boldsymbol{\delta}^{\mathrm{T}}\begin{bmatrix}\mathbf{K} \\ \mathbf{C}\end{bmatrix}^{\mathrm{T}}\begin{bmatrix}\widehat{\boldsymbol{\eta}} \\ \widehat{\boldsymbol{\psi}}\end{bmatrix}. \tag{54}$$

4. Simulation Results

To demonstrate the effectiveness and performance of the proposed attitude control schemes combined with RBFNN, a liquid-filled spacecraft model governed by equations (8a), (8b), (8c), and (11) is used to conduct numerical simulations. Neural network contains 15 nodes with center vector $\mathbf{c}$ evenly spaced in $[-\pi/6, \pi/6] \times [-\pi/6, \pi/6]$. Nominal inertia matrix of the spacecraft is given by

$$\mathbf{J} = \begin{bmatrix}503 & 0 & 0 \\ 0 & 385 & -5 \\ 0 & -5 & 420\end{bmatrix}\left(\mathrm{kg/m^2}\right). \tag{55}$$

The external disturbances are assumed to be

$$\mathbf{d}(t) = \begin{bmatrix}0.02\sin(0.1t) + 2 \\ 0.03\cos(0.4t) + 3 \\ 0.03\sin(0.3t) + 1\end{bmatrix}, \tag{56}$$

and an uncertainty $\Delta\mathbf{J}$ on the inertia matrix $\mathbf{J}$ is given by $\Delta\mathbf{J} = 0.5\mathbf{J}$; sensor noise is set as 0.5 rand (3, 1), where 0.5

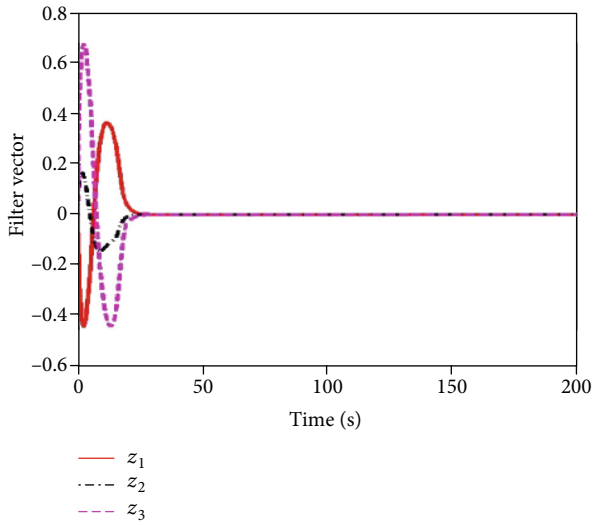

Figure 13: Time histories of filter vector in Case 2.

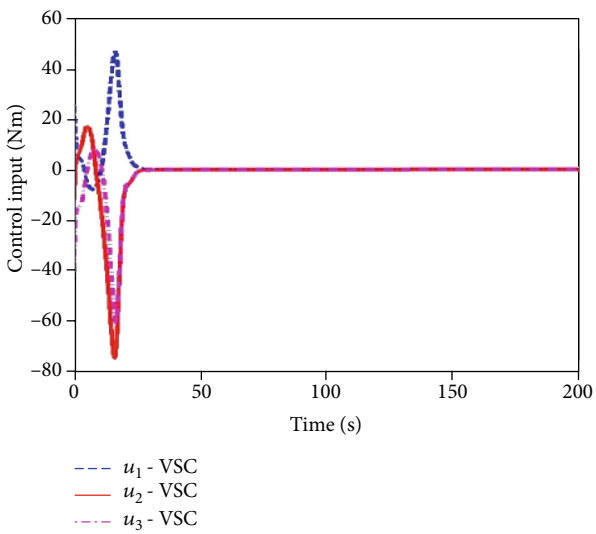

Figure 14: Time histories of control input in Case 2.

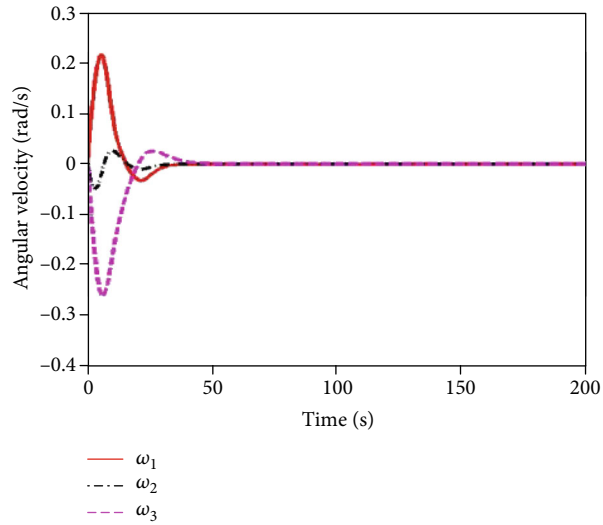

Figure 15: Time histories of angular velocities in Case 3 when $k(0) = 0.5$.

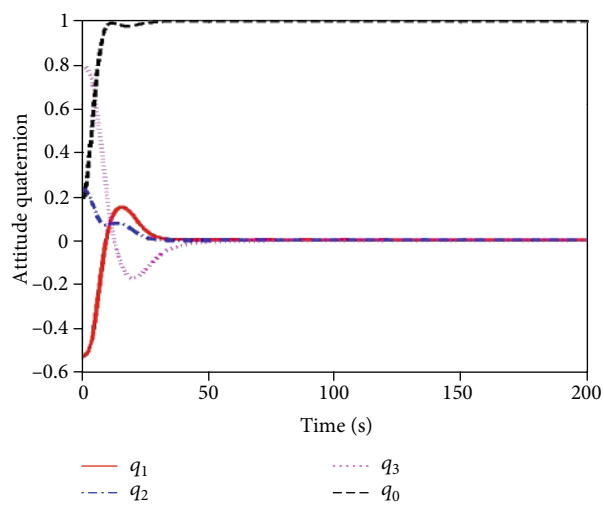

Figure 16: Time histories of attitude quaternions in Case 3 when $k(0) = 0.5$.

rand (3, 1) represents the random Gaussian white noise vector. The controller gains are listed as $k_p = 20$, $k_q = 5$, $k_z = 10$, $k_1 = 2$, $\mathbf{P} = 30\mathbf{I}_{15}$, $L_1 = L_2 = L_3 = 10$, $\sigma = 2$, $\gamma = 0.01$, $\mathbf{Q} = \mathbf{I}_4$, and $\delta_\theta = 0.05$.

The relevant parameters of liquid fuel sloshing are selected as $m_b = 100\text{kg}$, $m_p = 0.1m_b$, $l = 0.228\text{m}$, $r_x = 1.2\text{m}$, and $c_1 = c_2 = 0.05$. It is assumed that the spacecraft is at the earth's orbit altitude of 800 km and the local gravitational acceleration is selected as $g = 7.689\text{m/s}^2$.

Initial angular velocity is $\boldsymbol{\omega}(0) = [0 \quad 0 \quad 0]^{\mathrm{T}}$, initial displacement of the pendulum is $\widehat{\boldsymbol{\eta}}(0) = [0 \quad 0]^{\mathrm{T}}$, and initial quaternions value is

$$[q_0 \quad \mathbf{q}]^{\mathrm{T}} = [0.1736 \quad -0.5264 \quad 0.2623 \quad 0.7876]^{\mathrm{T}}. \tag{57}$$

Initial estimated neural network optimal weight is given by $\widehat{\boldsymbol{\theta}}(0) = [0, 0, 0]^{\mathrm{T}}$, and initial attitude gain is given by $k(0) = 2.5$. Bound of control torque is $u_m = 30\text{Nm}$.

To demonstrate the characteristics of the proposed control, three simulation cases are given below.

Case 1. Attitude maneuver control using variable structure output feedback control and RBFNN technique, the simulation results are shown in Figures 2–8.

Case 2. Attitude maneuver control using variable structure controller without considering RBFNN, the simulation results are shown in Figures 9–14.

The simulation results of Case 1 are shown in Figures 2–8. The simulation results of Case 2 are shown in Figures 9–14. Figures 2 and 9 show the time histories of angular velocities.

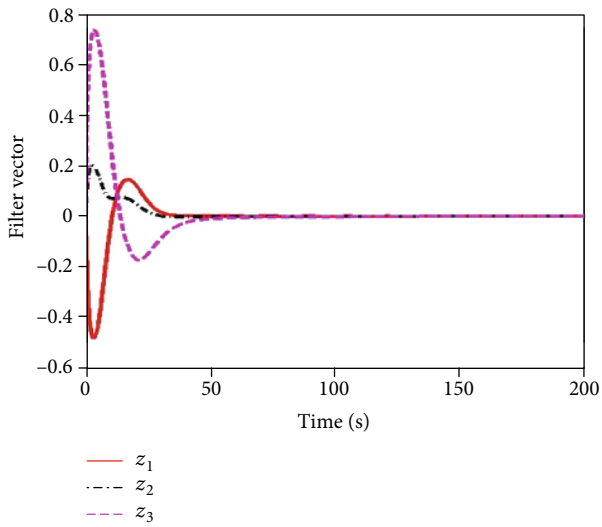

Figure 17: Time histories of filter vector in Case 3 when $k(0) = 0.5$.

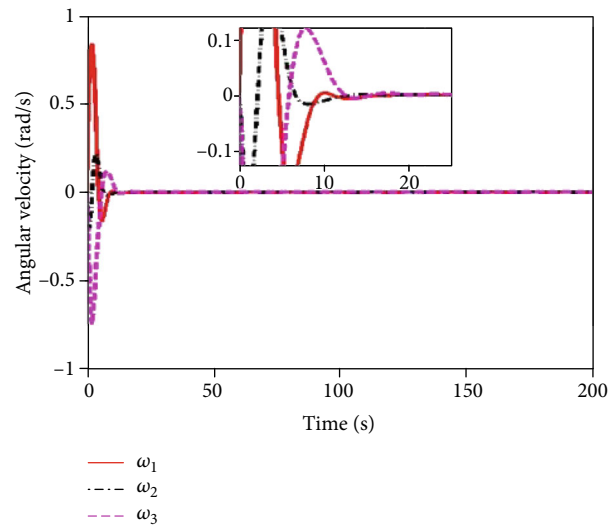

Figure 19: Time histories of angular velocities in Case 3 when $k(0) = 5$.

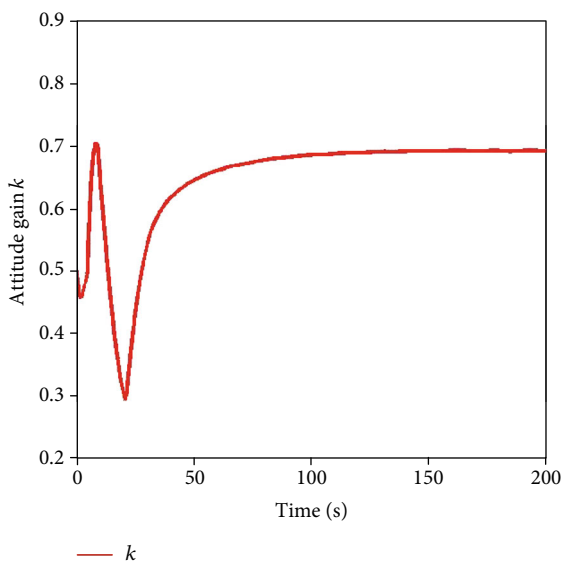

Figure 18: Time histories of attitude gain k in Case 3 when $k(0) = 0.5$.

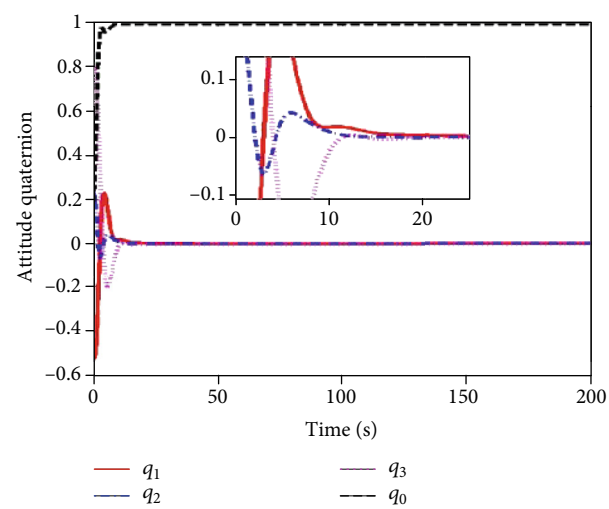

Figure 20: Time histories of attitude quaternions in Case 3 when $k(0) = 5$.

Figures 3 and 10 show the time histories of the quaternions. Compared with Figures 9 and 10, it can be observed from Figures 2 and 3 that the angular velocities and quaternions converge to the origin in around 20 seconds with good performance and smooth transient response. This demonstrates that the proposed robust control law incorporated with RBFNN can accomplish the desired attitude maneuver under the influence of external disturbances, parametric uncertainty, and sensor noise. Figure 4 shows the time histories of the liquid sloshing displacement. It can be seen that the liquid sloshing displacement is low amplitude from Figure 4. Specifically, the sloshing amplitude is less than 0.1 m. This indicates that the proposed controller can successfully account for the effect of liquid sloshing on the attitude maneuver ability of spacecraft. Figure 5 presents the time histories of attitude gain k. It can be reported from Figure 5 that the control objective is achieved and $k(t)$ converges to approximately 0.5 in about 60 seconds.

Figures 6 and 12 show the time histories of the filter state. In contrast to Figure 12, the state of the filter also converges to the origin with good transient and steady-state response performance from Figure 6. This demonstrates that the proposed filter is stable and can effectively reject the influence of the sensor noise to ensure the stability of the overall system. Figure 7 shows the time history of the estimated RBFNN optimal weight. It can be seen from Figure 7 that the estimated optimal weight state also converges to zero with good transient and smooth response performance. This shows that the RBFNN saturation compensator is stable and can effectively compensate for saturation nonlinearity. Figures 8 and 14 report the control torques with the RBFNN saturation

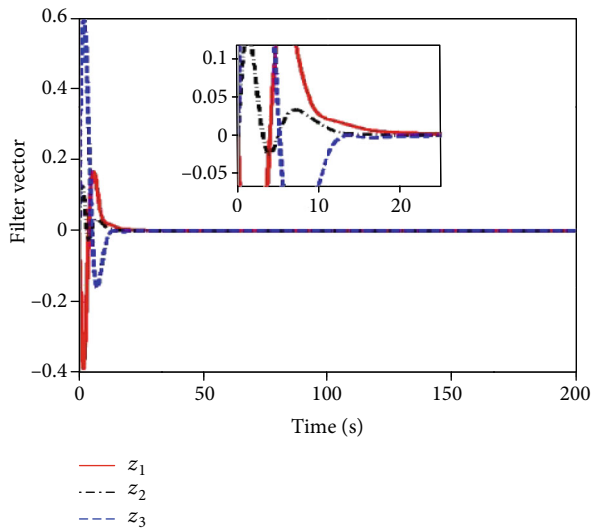

Figure 21: Time histories of filter vector in Case 3 when $k(0) = 5$.

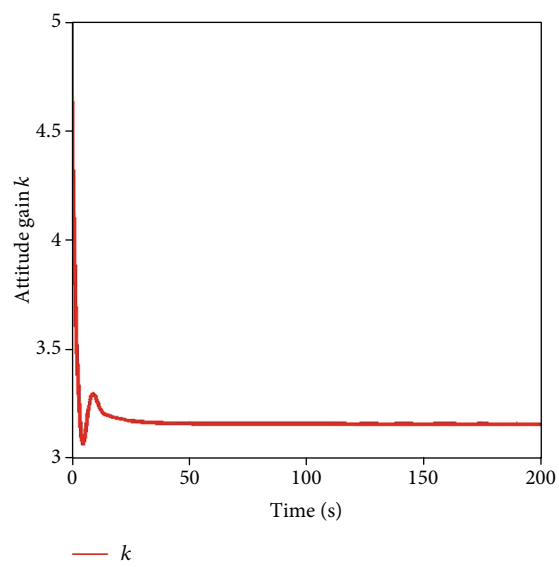

Figure 22: Time histories of attitude gain k in Case 3 when $k(0) = 5$.

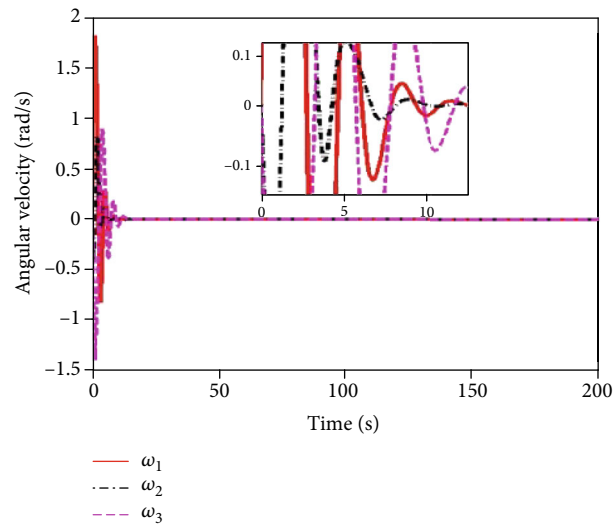

Figure 23: Time histories of angular velocities in Case 3 when $k(0) = 10$.

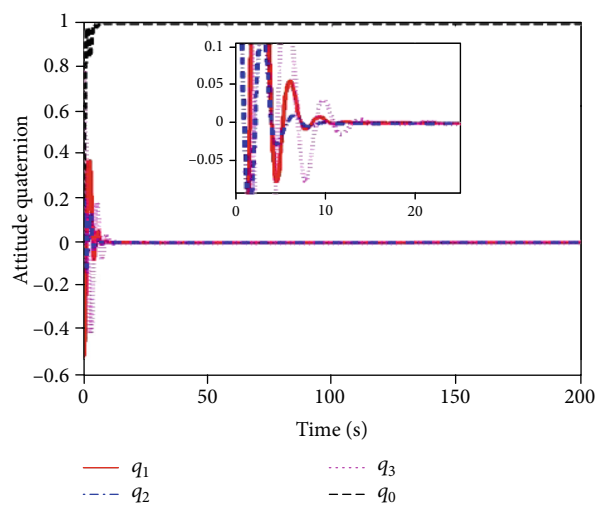

Figure 24: Time histories of attitude quaternions in Case 3 when $k(0) = 10$.

compensator and without the RBFNN saturation compensator, respectively. It can be seen that all three components of the control signals with the RBFNN saturation compensator exceed the control signals without RBFNN saturation compensator. The energy consumption indicator $E_n = \int_0^t \|\mathbf{u}(t)\| dt$ is introduced here and is calculated over the total simulation time of $t = 200$s. It is obvious that the robust saturated control strategy completes the attitude maneuver successfully with less control energy.

Case 3. The roles of auxiliary function $k(0)$ on the system response are demonstrated by choosing three different initial $k(0)$ values. The simulation results are shown in Figures 15–18 by choosing $k(0) = 0.5$. The simulation results are shown in Figures 19–22 by choosing $k(0) = 5$. The simulation results are shown in Figures 23–26 by choosing $k(0) = 10$.

The simulation results are shown in Figures 15–18 by choosing $k(0) = 0.5$, the simulation results are shown in Figures 19–22 by choosing $k(0) = 5$, and simulation results are shown in Figures 23–26 by choosing $k(0) = 10$. Here, the role of attitude gain $k(0)$ is explained in the language of classical second-order linear system. A smaller $k(0)$ value is conceptually equivalent to a higher damping ratio. When $k(0)$ value decreases, the emphasis of control will deviate from the $\mathbf{q}$ term and move towards the $\boldsymbol{\omega}$ term, which will lead to overdamped sluggish behavior in Figures 15–18. The higher $k(0)$ value corresponds conceptually to the lower damping ratio. When k increases, the focus of control is shifted away from $\boldsymbol{\omega}$ term and moves towards $\mathbf{q}$ term, which results in the underdamped oscillation behavior shown in Figures 19–26. Therefore, $k(0)$ acts as desired weighting to achieve the acceptable response between angular velocity

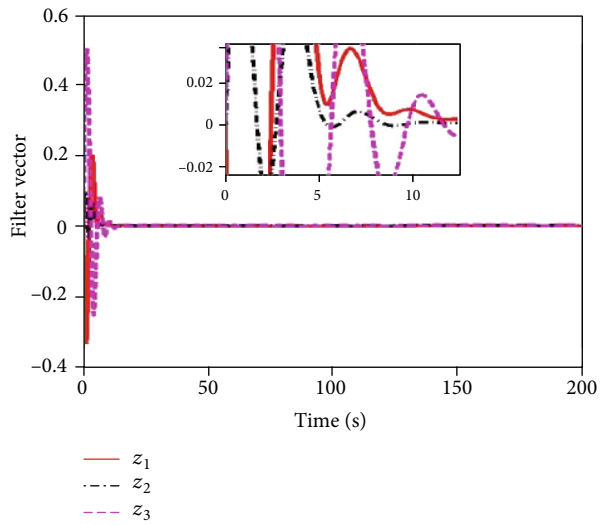

Figure 25: Time histories of filter vector in Case 3 when $k(0) = 10$.

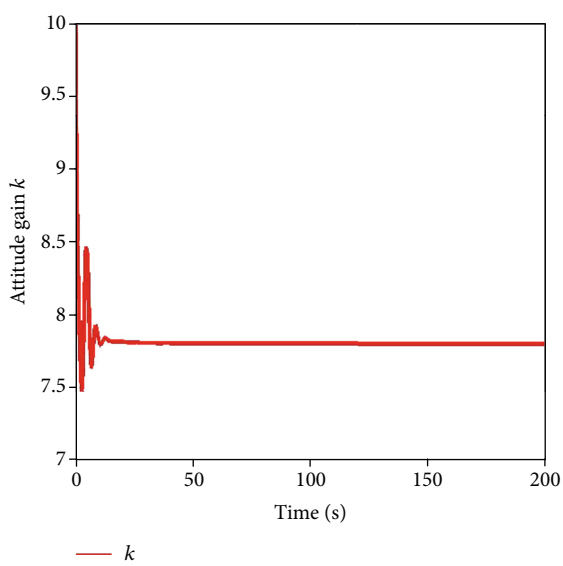

Figure 26: Time histories of attitude gain k in Case 3 when $k(0) = 10$.

$\boldsymbol{\omega}(t)$ and quaternions $\mathbf{q}(t)$, and these analyses are consistent with the explanation in Remark 12. Designers can appropriately choose $k(0)$ value and parameter γ to obtain acceptable transient and steady-state response performance and avoid slow or wild oscillation behavior.

5. Conclusions

In this paper, adaptive output feedback VSC is proposed for liquid- filled spacecraft attitude stabilization maneuver under control input saturation, parametric uncertainty, and bounded external disturbances. This control algorithm is based on the variable structure control and adaptive control technique. Additionally, this control algorithm uses continuous hyperbolic tangent functions to guarantee smoothness of the control signals and improve the transient response in the presence of parametric uncertainty and bounded external disturbances. Moreover, the problem of control input saturation is compensated based on RBFNN approaches, where an intelligent saturation compensator is inserted into a feedforward loop. Moreover, this control scheme uses a low-pass filter variable synthesized through a first-order stable differential equation, which is tuned by the filter parameter k_1 and driven by the sliding mode vector, and the influences of noisy measurements on the system response can be reduced by using this filter. Lyapunov analysis is employed to ensure global stability of the resulting closed-loop system. The asymptotic convergence of the system state variables is guaranteed by using Barbalat's lemma. Numerical examples are presented to illustrate the effectiveness and robustness of the proposed control method.

Data Availability

All the data used to support the findings of this study are available from the corresponding author upon request.

Conflicts of Interest

The authors declare that there is no conflict of interests regarding the publication of this paper.

Acknowledgments

The authors sincerely acknowledge the financial support of the National Natural Science Foundation of China (Grant Nos. 11962020, 11862020, and 11502122) and the Inner Mongolia Natural Science Foundation (Grant No. 2019MS05065).

References

[1] C. Nichkawde, P. M. Harish, and N. Ananthkrishnan, "Stability analysis of a multibody system model for coupled slosh–vehicle dynamics," *Journal of Sound and Vibration*, vol. 275, no. 3-5, pp. 1069–1083, 2004.

[2] H. N. Abramson, *The Dynamic Behavior of Liquids in Moving Containers*, Technical Report, NASA, Washington, DC, USA, 1966.

[3] S. Cho, M. McClamroch, and M. Reyhanoglu, "Feedback control of a space vehicle with unactuated fuel slosh dynamics," in *AIAA Guidance, Navigation, and Control Conference and Exhibit*, Dever, CO, USA, 2000.

[4] R. A. Ibrahim, *Liquid Sloshing Dynamics: Theory and Applications*, Cambridge University Press, 2005.

[5] B. Z. Yue, "Heteroclinic bifurcations in completely liquid-filled spacecraft with flexible appendage," *Nonlinear Dynamics*, vol. 51, no. 1-2, pp. 317–327, 2007.

[6] B. Z. Yue, "Study on the chaotic dynamics in attitude maneuver of liquid-filled flexible spacecraft," *AIAA Journal*, vol. 49, no. 10, pp. 2090–2099, 2011.

[7] B. Z. Yue and L. M. Zhu, "Hybrid control of liquid-filled spacecraft maneuvers by dynamic inversion and input shaping," *AIAA Journal*, vol. 52, no. 3, pp. 618–626, 2014.

[8] X. J. Song and S. F. Lu, "Attitude maneuver control of liquid-filled spacecraft with unknown inertia and disturbances,"

Journal of Vibration and Control, vol. 25, no. 8, pp. 1460–1469, 2019.

[9] H. Zhang and Z. Wang, "Attitude control and sloshing suppression for liquid-filled spacecraft in the presence of sinusoidal disturbance," *Journal of Sound and Vibration*, vol. 383, pp. 64–75, 2016.

[10] J. Y. Kang and J. E. Cochran, "Resonant motion of a spin-stabilized thrusting spacecraft," *Journal of Guidance, Control, and Dynamics*, vol. 27, no. 3, pp. 356–365, 2004.

[11] J. D. Boškovic, S. M. Li, and R. K. Mehra, "Robust adaptive variable structure control of spacecraft under control input saturation," *Journal of Guidance, Control, and Dynamics*, vol. 24, no. 1, pp. 14–22, 2001.

[12] R. J. Wallsgrove and M. R. Akella, "Globally stabilizing saturated attitude control in the presence of bounded unknown disturbances," *Journal of Guidance, Control, and Dynamics*, vol. 28, no. 5, pp. 957–963, 2005.

[13] A. Sabanovic, "Variable structure systems with sliding modes in motion control—a survey," *IEEE Transactions on Industrial Informatics*, vol. 7, no. 2, pp. 212–223, 2011.

[14] J. Y. Hung, W. Gao, and J. C. Hung, "Variable structure control: a survey," *IEEE Transactions on Industrial Electronics*, vol. 40, no. 1, pp. 2–22, 1993.

[15] Q. Hu, "Variable structure maneuvering control with time-varying sliding surface and active vibration damping of flexible spacecraft with input saturation," *Acta Astronautica*, vol. 64, no. 11-12, pp. 1085–1108, 2009.

[16] Q. Hu and G. Ma, "Control of three-axis stabilized flexible spacecraft using variable structure strategies subject to input nonlinearities," *Journal of Vibration and Control*, vol. 12, no. 6, pp. 659–681, 2006.

[17] R. A. DeCarlo, S. H. Zak, and G. P. Matthews, "Variable structure control of nonlinear multivariable systems: a tutorial," *Proceedings of the IEEE*, vol. 76, no. 3, pp. 212–232, 1988.

[18] J. D. Boskovic, "A multiple model-based controller for nonlinearly-parametrized plants," in *Proceedings of the 1997 American Control Conference (Cat. No.97CH36041)*, pp. 2140–2144, Albuquerque, NM, USA, 1997.

[19] K. S. Narendra and J. D. Bošković, "Robust adaptive control using a combined approach," *International Journal of Adaptive Control and Signal Processing*, vol. 4, no. 2, pp. 111–131, 1990.

[20] A. M. Zou and K. D. Kumar, "Adaptive fuzzy fault-tolerant attitude control of spacecraft," *Control Engineering Practice*, vol. 19, no. 1, pp. 10–21, 2011.

[21] A. M. Zou and K. D. Kumar, "Neural network-based distributed attitude coordination control for spacecraft formation flying with input saturation," *IEEE transactions on neural networks and learning systems*, vol. 23, no. 7, pp. 1155–1162, 2012.

[22] Z. Zhu, Y. Xia, and M. Fu, "Adaptive sliding mode control for attitude stabilization with actuator saturation," *IEEE Transactions on Industrial Electronics*, vol. 58, no. 10, pp. 4898–4907, 2011.

[23] J. Ma, S. S. Ge, Z. Zheng, and D. Hu, "Adaptive NN control of a class of nonlinear systems with asymmetric saturation actuators," *IEEE transactions on neural networks and learning systems*, vol. 26, no. 7, pp. 1532–1538, 2015.

[24] W. Gao and R. R. Selmic, "Neural network control of a class of nonlinear systems with actuator saturation," *IEEE Transactions on Neural Networks*, vol. 17, no. 1, pp. 147–156, 2006.

[25] M. Chen, S. S. Ge, and B. V. E. How, "Robust adaptive neural network control for a class of uncertain MIMO nonlinear systems with input nonlinearities," *IEEE Transactions on Neural Networks*, vol. 21, no. 5, pp. 796–812, 2010.

[26] J. Zhou, "Adaptive neural network control of uncertain nonlinear plants with input saturation," in *2009 Chinese Control and Decision Conference*, pp. 23–28, Guilin, China, 2009.

[27] M. Li, M. Hou, and C. Yin, "Adaptive attitude stabilization control design for spacecraft under physical limitations," *Journal of Guidance, Control, and Dynamics*, vol. 39, no. 9, pp. 2179–2183, 2016.

[28] Q. Hu and B. Xiao, "Intelligent proportional-derivative control for flexible spacecraft attitude stabilization with unknown input saturation," *Aerospace Science and Technology*, vol. 23, no. 1, pp. 63–74, 2012.

[29] V. Utkin, "Variable structure systems with sliding modes," *IEEE Transactions on Automatic Control*, vol. 22, no. 2, pp. 212–222, 1977.

[30] H. Sun, L. Hou, G. Zong, and L. Guo, "Composite anti-disturbance attitude and vibration control for flexible spacecraft," *IET Control Theory & Applications*, vol. 11, no. 14, pp. 2383–2390, 2017.

[31] M. R. Akella, A. Valdivia, and G. R. Kotamraju, "Velocity-free attitude controllers subject to actuator magnitude and rate saturations," *Journal of Guidance, Control, and Dynamics*, vol. 28, no. 4, pp. 659–666, 2005.